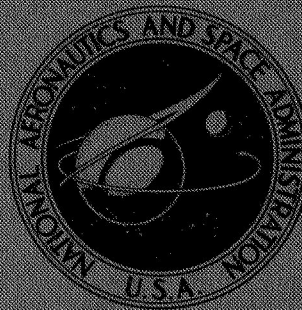


NASA TECHNICAL
MEMORANDUM



N73-30749
NASA TM X-2863

NASA TM X-2863

CASE FILE
COPY

TRANSIENT ANALYSIS OF
ENERGY TRANSFER CONTROL (ETC)
AND COMPRESSOR BLEED CONCEPTS
OF REMOTE LIFT FAN CONTROL

by James F. Sellers

Lewis Research Center

Cleveland, Ohio 44135

1. Report No. NASA TM X-2863	2. Government Accession No.	3. Recipient's Catalog No.	
4. Title and Subtitle TRANSIENT ANALYSIS OF ENERGY TRANSFER CONTROL (ETC) AND COMPRESSOR BLEED CONCEPTS OF REMOTE LIFT FAN CONTROL		5. Report Date September 1973	
		6. Performing Organization Code	
7. Author(s) James F. Sellers		8. Performing Organization Report No. E-7437	
		10. Work Unit No. 501-24	
9. Performing Organization Name and Address Lewis Research Center National Aeronautics and Space Administration Cleveland, Ohio 44135		11. Contract or Grant No.	
		13. Type of Report and Period Covered Technical Memorandum	
12. Sponsoring Agency Name and Address National Aeronautics and Space Administration Washington, D. C. 20546		14. Sponsoring Agency Code	
		15. Supplementary Notes	
16. Abstract The transient performance of two concepts for control of VTOL aircraft remote lift fans is analyzed and discussed. Both concepts employ flow transfer between pairs of lift fans located in separate parts of the aircraft in order to obtain attitude control moments for hover and low-speed flight. The results presented are from a digital computer, dynamic analysis of the YJ97/LF460 remote drive turbofan. The transient responses of the two systems are presented for step demands in lift and moment.			
17. Key Words (Suggested by Author(s)) Vertical takeoff aircraft; J-97 engine; Engine control; Control; Turbofan engines; Lift fans		18. Distribution Statement Unclassified - unlimited	
19. Security Classif. (of this report) Unclassified	20. Security Classif. (of this page) Unclassified	21. No. of Pages 53	22. Price* \$3.00

* For sale by the National Technical Information Service, Springfield, Virginia 22151

TRANSIENT ANALYSIS OF ENERGY TRANSFER CONTROL (ETC) AND COMPRESSOR BLEED CONCEPTS OF REMOTE LIFT FAN CONTROL

by James F. Sellers

Lewis Research Center

SUMMARY

This report discusses the transient performance of two control concepts for VTOL aircraft remote lift fan systems: the Energy Transfer Control (ETC) concept and a compressor-bleed concept. The compressor-bleed concept is new and has not been covered in previous literature. Both systems employ cross ducting to permit flow transfer among pairs of lift units located in different parts of the aircraft. This method of control allows one unit to increase in thrust at the expense of the opposite unit, which is the ideal situation for attitude control of a hovering VTOL aircraft. The results presented are from a nonlinear digital simulation of the YJ97/LF460 remote drive turbofan. The YJ97/LF460 was chosen for study because it is proposed for use in a VTOL research aircraft.

The transient responses of the ETC and compressor-bleed systems are presented for step inputs simulating height and attitude control demands for a hovering VTOL aircraft. The dynamic characteristics of each system are discussed and comparison is made with VTOL thrust response criteria. Both systems are shown to have good potential for meeting the requirements of a VTOL aircraft lift system.

INTRODUCTION

Vertical takeoff and landing (VTOL) aircraft have been the subject of continuing research over the past decade. Recent studies by NASA (refs. 1 to 3) have shown that commercial VTOL transports powered by turbofan engines show promise in meeting the requirements for a quiet, clean transportation system that is not dependent on long airport runways. In order to minimize the number of engines, proposed VTOL transports use the same engines for cruise propulsion, lift, and attitude control in hover.

The objective of this study was to determine whether new control concepts proposed for the VTOL application could successfully meet the transient response requirements imposed by the use of lift engines for attitude and height control. The YJ97/LF460 remote fan system was chosen for study because it is proposed for use in a VTOL research aircraft (refs. 1 to 3).

In a remote drive turbofan, a gas generator, such as the YJ97, supplies hot gas to drive a fan, such as the LF460. The gas generator and fan are separated by a duct and need not be coaxial. This permits flexibility of installation as illustrated in figure 1(a), which shows the YJ97/LF460 combination in two possible configurations. The LF460 fan is unconventional in the respect that the turbine blades are mounted about the circumference of the fan. This increases fan diameter but reduces the length.

Figure 1(b) shows how the YJ97/LF460 lift units are arranged in two proposed VTOL research transports (refs. 1 and 3) to provide lift, attitude control, and cruise propulsion.

For attitude control the ideal situation is to increase the thrust of one fan at the expense of the opposite fan. This situation can be realized with flow transfer between separate units. Various methods have been proposed to accomplish this, among them the Variable Area Scroll (VAS) concept (ref. 4), and the Turbine Energy Modulation (TEM) concept (ref. 5). Both of these systems are covered in the literature and will not be discussed here. The subjects of this report are two recent and promising control concepts: the Energy Transfer Control (ETC) system (ref. 6) and a compressor-bleed system.

The operating principles and steady-state performance of the ETC and compressor-bleed systems are detailed in references 6 and 7. The steady-state moment generating capabilities of both systems are very similar. Each concept employs unique means of recovering lift after gas-generator or fan failures; this aspect of their operation is also discussed in reference 7.

While steady-state performance and fail operational capability are essential areas of interest for both systems, their transient thrust response is also important. This report discusses the transient performance of each system, based on detailed dynamic simulations programmed for a digital computer. The symbols and equations used in the simulations are presented in appendixes A and B. The response of each system to step demands in collective lift (height control) and moment (attitude control) are presented, and the results are compared and discussed.

YJ97/LF460 STEADY-STATE PERFORMANCE

The YJ97 (ref. 8) is a single-rotor turbojet designed primarily for military applications. Preliminary design has been completed for the LF460 lift fan (ref. 9), which is intended for the low-noise commercial application. Since steady-state performance of

the YJ97/LF460 turbofan has been discussed in references 6, 7, and 9, only the design point performance will be given here as summarized in table I. The design point is here defined as a single YJ97 driving a single LF460 at the sea-level-static, standard-day condition. The YJ97 is at its military power setting (101.5 percent speed), and 100-percent inlet pressure recoveries are assumed. The data presented in this report are all normalized with respect to the design point data of table I.

PRINCIPLES OF OPERATION

In this section a brief description of the Energy Transfer Control (ETC) and compressor-bleed systems will be given to assist in explaining the transient analysis and results.

A schematic of the ETC system is shown in figure 2. Two gas generators and two fans are shown, plus a cross duct connecting the gas-generator exhaust ducts. Two butterfly valves are mounted just upstream of each fan scroll inlet. When no control moment is needed all valves are wide open and no crossflow occurs (fig. 2(a)). Both fans produce the same thrust, assuming identical performance.

When a control moment is requested (fig. 2(b)), the two butterfly valves upstream of the low-thrust-side fan turbine are rotated to a partly closed position, but the two high-side valves are left wide open. Assuming the gas generators to have constant-speed governors, the following effects occur: gas-generator exhaust flow is transferred from the low side to the high side through the cross duct; exhaust-gas pressure and temperature increase because of the flow restriction introduced by the partly closed valves; and high-side fan speed and thrust increase markedly because of the increased pressure, temperature, and flow.

Because of the partly closed valves, the low-side fan receives less flow than in the trim condition. However, the temperature increases while the pressure loss caused by the valves is offset by the increase in duct pressure. As a result, low-side fan speed and thrust remain nearly constant. Since the total thrust of the high- and low-side fans should remain constant compared with trim, some sort of thrust spoiling is needed on the low side. Spoiling is typically accomplished by louvers mounted in the fan exhaust stream, which are partly shut when a thrust loss is desired.

The compressor-bleed system is shown schematically in figure 3. The main difference between the ETC and compressor-bleed systems is that in the bleed system relatively cool compressor-bleed air flows through the cross duct, instead of gas-generator exhaust gas. The amount of compressor bleed is controlled by the bleed valves; the injection valves govern the amount of duct air injected into the hot stream between gas generator and fan. In the trim condition (fig. 3(a)) all valves are closed and no crossflow occurs. When a moment is requested, the valves are operated as shown in figure 3(b),

so that bleed flow from the low-side gas generator is injected into the exhaust duct on the high side.

The injection of bleed air into the high-side exhaust stream implies that more flow is passing through the fan turbine than in the trim condition. The increased flow rate further implies an increase in gas-generator back pressure; the gas generator governor, therefore, must increase the fuel flow rate to maintain constant speed. This fuel flow increase in turn causes an increase in gas-generator discharge temperature. Although the addition of bleed air cools the gas somewhat, the net effect on the high-side fan is very similar to what the ETC system produces: thrust and speed increase markedly because of higher flow, pressure, and temperature.

The results on the low side are also similar to those produced by the ETC system. The low-side fan receives less flow because air is being bled over to the high side. However, the fuel flow rate to the gas generator must increase to hold speed constant despite the high bleed rate. As a result, gas-generator turbine-inlet and turbine-discharge temperatures increase. The combination of lower flow at higher temperature causes the low-side fan to lose some thrust, but spoiling is still required to keep the total thrust of the two fans constant relative to the trim condition. The amount of spoiling required is less for the bleed system than for the ETC system. This turns out to have some effect on the transient response, as will be discussed in a later section.

The two systems are about equal in the amount of attitude control moment that they can produce. For the YJ97/LF460 system a thrust difference of over 26 700 N (6000 lbf) can be developed between two fans over a wide range of YJ97 power settings. This means a normalized thrust increase of 0.24 on the high side and a decrease of equal magnitude on the low side. This amount of control moment is adequate even for transport-size VTOL aircraft (refs. 1 to 3). By controlling the rate of flow transfer with the valves, the amount of control moment can be easily modulated. Furthermore, the total thrust of the two fans can be varied by changing gas-generator power setting, always keeping both gas generators at the same speed.

Both systems rely on the fact that large attitude control moments are only needed for short lengths of time during flight. When flow transfer is employed at the maximum power setting of the gas generator, short-duration overtemperatures occur. The YJ97 steady-state exhaust-gas temperature (EGT) limit is 1019 K (1835^o R), but the transient EGT limit applicable during flow transfer is 1144 K (2060^o R) (ref. 6). The YJ97 compressor stall margin (see eq. (B13) for definition) is also reduced during flow transfer: to about 0.15 at maximum moment from about 0.21 at trim. These effects are undesirable but still tolerable. A partial feasibility demonstration of the ETC system has already been made by running two interconnected YJ97's without fans (ref. 6). This demonstration showed that the YJ97 could indeed operate under these conditions without damage.

TRANSIENT RESPONSE CRITERIA

Research on VTOL aircraft has resulted in comprehensive handling qualities criteria (ref. 10). The criteria from reference 10 that apply to the thrust control system of a lift-fan aircraft are summarized below. For convenience, time constant τ shall be taken to mean the time to achieve 63 percent of a commanded step change in moment or lift, regardless of whether the response in question is actually a first-order lag. This usage is consistent with reference 10 and will be maintained throughout this report.

Moment response for attitude control: Attitude control moment, which is proportional to the thrust difference between opposed lift units, should have a time constant less than 0.20 second.

Thrust response for height control: Aircraft height control in hover is obtained by collective thrust modulation of the lift units. The time constant for this response should be less than 0.50 second. Furthermore, sufficient lift capability should be available to provide vertical accelerations of ± 0.10 g about some nominal hovering condition. This implies that the time constant requirement must be met for thrust modulations of ± 10 percent about the nominal level.

ANALYTICAL PROCEDURE

The results presented in this report were produced by a digital computer program that simulates the dynamics of the YJ97/LF460 system. A single basic program was used with appropriate modifications, depending on whether the ETC or compressor-bleed system was being studied. The analytical model included all major dynamics of an interconnected pair of lift units: two gas generators, including compressor, combustor, turbine, and fuel-control dynamics; cross ducting, valve, and actuator dynamics; and two fan units, including fan, fan turbine, and spoiler dynamics. Figure 4 shows how these components are arranged for each system. Also shown are the station designations used in the analysis. All symbols are defined in appendix A, and all equations are listed in appendix B.

Since the objective of this study was the identification of basic system dynamics, a simple control structure was used. The controls for the two systems were kept similar so that comparisons in transient performance could be made.

For the ETC system (fig. 5(a)) the pilot of the aircraft has control of two inputs: demand butterfly valve position $\theta_{v,dem}$ and demand YJ97 speed N_{dem} . Valve position determines the amount of attitude control moment generated, and speed demand controls the total thrust level for height control. The parameters that are measured and fed into the control system are actual YJ97 speed N_G , YJ97 compressor-inlet temperature T_2 , and YJ97 compressor-discharge static pressure P_{3S} .

As shown in figure 5(a), the butterfly valve actuator was modeled as a first-order lag with a 0.05-second time constant. The spoiler actuator was modeled in the same way. Demand spoiler angle β_{dem} was scheduled as a function of $\theta_{v,dem}$ and N_{dem} . As discussed earlier, spoiling of the low-side fan is needed to keep total lift constant during moment applications. The spoiler schedule for the ETC system is shown in figure 5(b); this schedule was selected to maintain steady-state total lift constant for a given YJ97 speed, regardless of attitude control moment.

Figure 5(a) also shows the YJ97 fuel control, which is an isochronous governor with acceleration and deceleration fuel flow limiting. The YJ97 was designed as a military turbojet, so the fuel control is not necessarily the best for this unconventional application. However, the YJ97 fuel control was modeled in its current form to see if any modifications were necessary. As shown in figure 5(a), closed-loop control of N_G is maintained. The dynamics of the fuel control were simulated by a transfer function. The time constants τ_2 and τ_3 are small, so the response of fuel flow \dot{w}_f to speed error N_{err} is essentially proportional-plus-integral. If N_{err} is large, for example, during an acceleration from idle to full power, the acceleration schedule will limit the rate of fuel flow delivered to the combustor. This limiting action is designed to prevent over-temperatures and compressor stall. A limit parameter $(\dot{w}_f/P_3)_{accel}$ is computed as a function of N_G and T_2 . This parameter is then multiplied by P_{3S} to obtain an upper limit on fuel flow $(\dot{w}_f)_{accel}$. A lower limit $(\dot{w}_f)_{decel}$ is also computed to prevent combustor blowout during severe decelerations. (The form of the acceleration schedule is shown in fig. 21.)

Figure 6(a) shows the controls for the compressor-bleed system, which are very similar to those for the ETC system. The pilot inputs remain the same: valve position for moment control and YJ97 demand speed for height control. However, valve position in this case is demand bleed valve area $A_{B,dem}$. The bleed and injection valves were modeled as variable-area orifices (see eqs. (B58 to (B63)). Each bleed valve was assumed to be connected to the injection valve on the opposite side. The opposite injection valve area was always set to twice the area of the bleed valve. This was done so that at steady-state the injection valve would be unchoked and the bleed valve choked. As a result the amount of crossflow depended only on YJ97 speed and bleed-valve area A_B . This dependence is illustrated in figure 6(b). Spoiler angle β was also scheduled as a function of A_B and YJ97 speed, again using the criterion that steady-state total lift should not depend on the amount of moment generated. The spoiler schedule is shown in figure 6(c). The YJ97 fuel control was modeled in exactly the same way as for the ETC system.

All the analytical results presented in this report assume sea-level-static, standard-day conditions. For study purposes the design point summarized in table I was chosen to represent the takeoff condition for a fully loaded aircraft, and 92 percent YJ97 speed was

chosen as the nominal power setting for approach and landing at minimum aircraft weight. The YJ97/LF460 produces 56.4 percent of design thrust at this YJ97 speed.

TRANSIENT PERFORMANCE

As discussed in the previous section, the ETC and compressor-bleed systems have separate inputs for the control of moment and collective lift. The transient responses are different for these two kinds of inputs, so they will be discussed separately.

Collective Lift Response

For multiengine aircraft of the type shown in figure 1(b), height control can be accomplished by collectively changing the speed demand to all the gas generators. In the trim condition this involves no crossflow between connected lift units. As a result the ETC and bleed systems have identical performance for this type of input.

The lift response will first be examined for step changes of maximum size. According to the response criteria mentioned earlier, the maximum step size would correspond to an aircraft vertical acceleration change of -0.10 g to $+0.10$ g. Figure 7(a) shows the response of the YJ97/LF460 to a step change in demand lift from 0.80 to 1.00 and from 1.00 back to 0.80. (Thrust is normalized with respect to the value in table I.) This lift change is accomplished by stepping YJ97 demand speed from 95.8 percent to 101.5 percent and back to 95.8 percent. Assuming the aircraft to hover at a thrust level of about 0.90, this step size corresponds to the maximum ± 0.10 -g variation in aircraft acceleration. As shown by figure 7(a), the time constant τ for the thrust increase is 0.25 second, and the time constant for the decrease is 0.30 second. Both responses are satisfactory ($\tau < 0.5$ sec) according to the criterion of reference 10.

The previous result is for cases near maximum thrust, such as would occur during takeoff. The response of the YJ97/LF460 becomes slower, however, as the initial power setting of the YJ97 is lowered. Figure 7(b) demonstrates this fact. Thrust demand is stepped from 0.564 to 0.680 and back to 0.564; that is, the YJ97 speed demand is stepped from 92 percent to 93.9 percent and back to 92 percent. Assuming a hovering thrust level of 0.622, these step sizes again correspond to aircraft accelerations of ± 0.10 g. The time constants for the increasing and decreasing thrust case are, respectively, 0.52 and 0.54 second. These responses are marginal with respect to the criterion of reference 10.

The trend toward slower response at lower thrust levels is summarized in figure 8. Time constant is plotted against initial thrust level with step size as a parameter. A positive step size means a lift increase, while a negative step signifies a decrease.

Time constant varies sharply with initial thrust level and to a lesser degree with step size. The transient response is marginal for initial lift levels below about 0.90.

According to the analysis, the acceleration and deceleration schedules in the YJ97 fuel control (figs. 5 and 6) had no effect on the responses shown in figures 7 and 8. That is, the proportional-plus-integral speed governor never produced fuel flows large enough to impinge on engine protective limits. The reason for this is that the maximum step sizes for the VTOL application are still quite small compared with, say, a throttle slam from idle to military power. It is reasonable to assume that a redesigned governor could be made more sensitive to small speed errors and hence improve the lift response for the VTOL application, since margin is still available before engine limits are encountered. Another plausible way to improve the lift response is by means of spoiling. The engines could be run at a thrust level higher than necessary for hover, and all thrust modulation for height control could be obtained by spoiling, which has a very fast response. In any case the lift response of the YJ97/LF460 system is already near satisfactory levels.

Moment Response

This section discusses the response of the ETC and compressor bleed systems to demands for attitude control moments. In flight, moment demands will vary continuously. Also, gas-generator speed demands will vary continuously for height control. However, for study purposes the response of each system to valve steps at constant speed demand will be discussed first. Simultaneous valve and throttle movements will be covered in a later section. The discussion will begin with a comparison of the two systems at the nominal takeoff condition (101.5 percent YJ97 speed). This is the flight condition where temperature and speed limits are most critical.

Figure 9 shows the response of the ETC system to a 33.5° step in valve position, at a demand YJ97 speed of 101.5 percent. This amount of valve movement results in the maximum steady-state moment that the ETC system can produce at this YJ97 speed (ref. 7). Figure 9(a) traces the time history of thrust for each LF460, as well as the sum and difference of the thrusts. The thrust increase on the high side is due to flow transfer; the decrease on the low side is primarily due to the action of the scheduled spoilers. The high-side fan responds rather slowly, with a time constant τ of 0.42 second. The spoiled fan responds much more quickly, with a τ equal to 0.09 second. Mainly because of the action of the spoiled fan, the moment response ($\tau = 0.19$ sec) is within the satisfactory range of τ less than 0.20 second (ref. 10).

The time history of normalized total thrust (net lift) in figure 9(a) shows the price paid for the fast moment response. The spoilers cause a transient drop in total lift with a minimum value of about 1.80; that is, about 10 percent less than the steady-state value

of 2.00. The importance of this drop will depend in part on how many engines the aircraft has. For example, a six-engine aircraft would only lose roughly 3.33 percent of its total lift from the transient shown in figure 9(a), assuming the other engines were operating continuously at full thrust. Furthermore, the drop only lasts about 1 second, which is not enough time for the aircraft to lose an appreciable amount of altitude. Finally, figure 9(a) is for the maximum amount of moment that the ETC system can produce. The lift loss for smaller moment demands would be proportionately less.

Figure 9(b) shows the speed responses for the two YJ97's and the two LF460's. Both YJ97's see a very similar disturbance in back pressure. Compared with the time scale of figure 9(b), the time delay introduced by the cross duct has a negligible effect. Also, the steady-state back pressures are the same except for a small pressure loss due to flow through the cross duct. Hence, the two YJ97's respond almost identically.

Quite different considerations explain the responses of the two LF460's. The high-side fan undergoes a large speed change, but the low-side fan loses relatively little speed. The transient histories are also quite different: the high-side response is slow with no overshoot; the low-side response is fast with a mild undershoot. The high-side fan has to depend on a flow, pressure, and temperature increase for its speed rise. Of these effects, the temperature rise is the slowest (fig. 9(c)); the cause of this will be discussed later. The low-side fan, on the other hand, is closely coupled to the valve just upstream of it and loses speed quickly when the valve acts to reduce the pressure and flow rate. The slow temperature rise is seen equally by both fans and causes the low-side fan to gradually rise to its final speed level. The low-side fan experiences a backpressuring effect because of the closing of spoilers in its exhaust stream, but this effect is quite small as far as the speed response is concerned. The primary effect of spoiling is on the thrust response (fig. 9(a)). An ideal spoiler would produce a thrust loss with no backpressuring at all, but obviously this would be difficult to realize in practice. For further detail on the spoilers assumed in this analysis, see equations (B88) to (B97).

Figure 9(c) traces the time history of YJ97 exhaust gas temperature (EGT). By considering the response of YJ97 speed (fig. 9(b)) along with the EGT response, the effect of the fuel control on overall system dynamics can be explained. Since the time delays due to the burner and turbine are quite small, EGT gives a good indication of what fuel flow is doing with respect to time.

Conventional turbojet control systems like the one used on the YJ97 depend on speed sensing to correct for back pressure effects. Hence, the dynamics of the gas-generator rotor and fuel control dominate the response to an increase in back pressure. This is what explains the slow rise in duct temperature and the slow increase in the speed of the high-side fan. The process of losing gas-generator speed takes time (as shown by fig. 9(b)). The YJ97 fuel control, sensing this speed loss, adds fuel to bring the speed back up to its steady-state level of 101.5 percent. The proportional-plus-integral action

of the YJ97 fuel control can be clearly seen in the EGT history: the initial peak is due to the fuel flow proportional to speed error; later on, the integral action dominates and gradually increases EGT to its final value. The initial peak does not exceed the final value, so the transient EGT limit is not exceeded.

In figure 9(d) the time history of YJ97 compressor stall margin (eq. (B13)) is shown. The significance of this figure is that stall margin does not overshoot its final value; therefore, stall problems are not necessarily worse than would be uncovered by a steady-state analysis.

In summary, the moment response of the ETC system is governed by two prominent factors: the slow response of the gas-generator governor and the fast response of the spoiled fan. Together, they result in satisfactory moment response at the expense of a transient net lift loss.

Figure 10 shows the response of the compressor-bleed system to a step demand in bleed-valve area of 19.1 square centimeters (2.95 in.²) at 101.5 percent YJ97 speed. This results in the maximum moment that the bleed system can produce at this YJ97 speed. Since the ETC and bleed systems have the same moment production capability (ref. 7), figures 9 and 10 can be compared directly. The thrust responses shown in figure 10(a) are qualitatively similar to those shown for the ETC system, but the time constants are different. The following table summarizes these differences:

	Time constant, τ , sec		
	High side	Low side	Moment
Bleed system	0.30	0.12	0.23
ETC system	.42	.09	.19

The bleed system responds faster on the high side, but slower on the low side. The net result is a slower moment response but less transient net lift loss.

Figure 10(b) helps to explain these differences. First of all, comparison with figure 9(b) shows that the low-side fan ends up at a lower speed in the bleed system than in the ETC system. This implies that the bleed system requires less spoiling, as mentioned in an earlier section. Therefore, the low-side thrust response is dominated to a lesser degree by spoiling and is slower as a result.

Figure 10(b) also shows that the two YJ97's do not respond identically, as in the ETC system. The low-side YJ97 response is governed by the the flow loss due to compressor bleed, rather than the effect of increased back pressure. The high-side YJ97 undergoes a greater transient speed loss than is the case with the ETC system. This greater speed loss is due to the high initial pressure in the cross duct. The injection rate of duct air into the high-side exhaust stream is initially high and then decays to its final value as the

duct pressure approaches equilibrium. This high initial flow rate results in a higher transient back pressure than in the ETC system and thus a greater YJ97 transient speed loss. This fact is also reflected in the YJ97 EGT time history shown in figure 10(c). The proportional action of the YJ97 fuel control causes a temperature overshoot for the high-side YJ97. This would be unacceptable in practice because the peak value exceeds the transient EGT limit. An EGT limiter in the YJ97 fuel control, which was not included in this analysis, would cure this problem at the expense of slowing the bleed system's response at near maximum moment demands. The rarity of maximum moment demands in flight reduces the impact of this type of transient performance limitation.

Figure 10(d) shows the time history of YJ97 compressor stall margin. The high-side YJ97 loses stall margin, while the low side gains. No serious overshoots occur before the final values are reached.

Qualitative conclusions about transient response for the bleed system are similar to those for the ETC system. The two dominating factors are the YJ97 governor and rotor dynamics and the spoiled thrust response. Neither system appears to have conclusive superiority in transient performance. Although the bleed-system's moment response is slower, its high-side thrust response is faster. This type of situation can always be improved by applying lead compensation to the spoilers and trading moment response for more transient lift loss.

So far the discussion of moment response has been confined to the nominal takeoff condition. However, the moment response, like the net lift response, varies as a function of YJ97 power setting.

Figures 11 and 12 show the responses for the ETC and bleed systems at 92 percent YJ97 speed, which is the nominal landing condition chosen for this study. Step valve demands are the same size as for figures 9 and 10. The responses are qualitatively similar to the 101.5 percent speed condition, but they are notably slower. Moment time constant is 0.25 second for the ETC system and 0.26 second for the bleed system; both are unsatisfactory according to the criterion of reference 10.

The unsatisfactory responses shown in figures 11 and 12 strengthen the statement that the YJ97 governor and rotor dynamics are of primary importance in overall system dynamics. The marginal lift responses shown in figure 7 for the landing condition are an aspect of the same problem illustrated by figures 11 and 12, namely, the slow response of the YJ97 to small speed errors at low power settings. This type of transient response was not a requirement in the design of the YJ97 fuel control, which performs satisfactorily according to military criteria.

Figure 13 summarizes the effect of initial thrust level on moment response time constant for both systems. The effect of step size is also included. Response degrades progressively as lift level is reduced from its maximum value of 1.00. The effect of step size is fairly weak. It should be kept in mind that the control systems used in this analysis included no lead compensation or other means of quickening the moment

response; an extensive control study was considered beyond the scope of this report. As discussed earlier, most of the response problem is due to a fuel control design that was not intended for this application. An anticipation loop could easily be provided in the YJ97 fuel control that would add an increment of fuel flow proportional to control valve position. This modification was analyzed in reference 11, and it gave satisfactory moment response at 92 percent YJ97 speed for both the ETC and compressor bleed systems. Additional study ought to reveal other modifications that would bring both systems closer to their full potential.

The step responses of the ETC and compressor-bleed systems are not the only transients of interest. That these systems are nonlinear is demonstrated by figures 14 and 15, which show the response of each system for sinusoidally varying moment demands at a frequency of 1 hertz. The YJ97 demand speed is held constant at 92 percent. When the moment demand is positive, one of the bleed or butterfly valves is actuated; for negative moments the opposite valve is actuated. As always, spoilers follow their schedules as a function of demand valve position and demand YJ97 speed.

The nonlinearity of the response shows up clearly in the total thrust trace in figure 14. The oscillations in total thrust occur at twice the frequency of the input, mainly because of the action of the spoilers, which cause a thrust drop for both positive and negative moments. The mean total thrust level, however, remains near its initial value because of a mean duct temperature rise caused by the YJ97 fuel control. A fuel flow higher than the trimmed level is required to maintain speed in the presence of continuous backpressure disturbances. Hence, in the presence of continuous moment demands, mean YJ97 EGT will be higher than its trimmed level for that power setting. Moment demands of either polarity always drive the gas generators towards higher temperatures and lower stall margins.

The same conclusions hold for the bleed system response shown in figure 15, with the exception that the high-side thrust peaks more nearly balance the effects of spoiling on the low side. As a result, total lift variations are smaller.

Simultaneous Lift and Moment Demands

The previous sections discussed transients associated with separately demanded collective lift changes and attitude control moments. In flight these demands will occur simultaneously. Although the exact nature of pilot inputs must be determined from piloted simulator studies, the following discussion shows the interactions that can occur during simultaneous step demands.

Figures 16 and 17 show ETC and bleed system responses to simultaneous throttle and valve steps. The step sizes were chosen to produce maximum allowable lift and moment changes; that is, a simultaneous vertical acceleration from -0.10 to ± 0.10 g, and

a normalized moment of 0.48 at the nominal takeoff condition. A transient of this severity would probably never be required in flight, but it was examined as a limiting case.

The ETC system moment response (fig. 16(a)) has a time constant of 0.22 second. Referring to figure 13, this is roughly what one would expect for a moment transient at constant YJ97 speed and at an initial lift level of 0.80. In other words, the net lift transient in figure 16(a) does not noticeably degrade the moment response.

The net lift response, however, has been degraded by the presence of the moment transient. For an isolated lift input (fig. 7) the time constant was 0.25 second; in figure 16(a) the time constant for the same step size has become 0.60 second. The reason for this is fairly obvious: because of the fast response of the spoilers, the net lift transient is initially in the wrong direction. It should be remembered, however, that in a multiengine aircraft other lift units will be receiving the command to increase thrust. Figure 16(a) only applies to two engines, and so presents a pessimistic picture. Nonetheless, transient moment-lift interactions do occur and may be a factor in aircraft handling qualities.

Figures 16(b) and (c) show that transients in YJ97 EGT and stall margin are slightly more severe for combined inputs than for separate inputs. The EGT overshoots the transient limit, and the stall margin undershoots its final value. Fuel flow very briefly hits the acceleration limit schedule during the early stages of the transient. This is generally encouraging, since the acceleration limit would probably not be a factor in transients of a more realistic size.

Similar conclusions may be drawn from the compressor bleed system transient shown in figure 17. Moment response ($\tau = 0.24$) is not significantly different from what would be expected for an isolated input. Net lift response ($\tau = 0.48$) is degraded to a lesser degree than for the ETC system. The penalty for this improvement shows up in the EGT and in the compressor stall margin, which peak at values slightly less favorable than for the ETC system. Again, YJ97 acceleration schedule enters into the early part of the transient.

In summary, both systems show unfavorable effects when severe lift and moment demands are combined. Moment response time is only a weak function of net lift demands, but net lift response can be strongly affected by moment demands. Furthermore, temperature and stall problems are more serious than for separate inputs.

CONCLUSIONS

A transient analysis was performed for two systems of VTOL aircraft lift fan control: Energy Transfer Control (ETC) and a compressor-bleed system. The compressor-bleed system is new and has not been analyzed in earlier literature. The YJ97/LF460

turbofan was simulated in this analysis because it is proposed for use in a VTOL research aircraft.

Compared with traditional turbofan control criteria, the VTOL thrust response requirements are quite severe: moment response should have a time constant less than 0.20 second, and total thrust response should have a time constant less than 0.50 second.

Response of the ETC and compressor bleed systems approached or met the requirements, even though an unsophisticated control system was assumed. Response times became slower as the thrust level of the system was lowered. For YJ97 power settings between 92 percent (landing) and 101.5 percent (takeoff), the net lift response of the YJ97/LF460 had time constants ranging from 0.25 to 0.54 second. For the same range of power settings, the moment response time constant for the ETC system varied from 0.19 to 0.25 second. Moment response time constant for the bleed system varied from 0.23 to 0.26 second. Both systems obtained fast moment response through the use of thrust spoiling, which produces a transient net lift loss. This effect was shown to degrade the net lift response when moment and net lift inputs were combined.

Neither system has conclusive superiority in response time. For all cases the conventional YJ97 governor had an important effect on overall system response. A conventional governor is not ideal for this application and must be modified to realize the full transient performance potential of the ETC and compressor-bleed systems. While improvements in response time are desirable, neither system revealed any problem areas that would disqualify them from future considerations.

Lewis Research Center,
National Aeronautics and Space Administration,
Cleveland, Ohio, June 13, 1973,
501-24.

APPENDIX A

SYMBOLS

A	area
a_i	constant
b_i	constant
C_f	friction coefficient
C_p	constant pressure specific heat
C_V	constant volume specific heat
C_{VL}	velocity coefficient
C_w	flow coefficient
e	internal energy
F	thrust
$\mathcal{F}_i()$	function
f()	unspecified function
g_c	gravitational conversion factor
h	enthalpy
I	polar moment of inertia
J	Joule's constant
K_i	control gain
K_L	torque conversion factor
K_N	speed conversion factor
L	torque
l	length
N	rotor speed
P	total pressure
q	dynamic pressure
R	ideal gas constant
S	Laplace transform variable
T	total temperature

t	time
u	velocity
V	volume
w	stored mass
\dot{w}	mass flow rate
β	spoiler angle
γ	specific heat ratio
Δ	incremental change
δ	pressure normalized to standard-day conditions
η	efficiency
θ	temperature normalized to standard-day conditions
θ_v	butterfly valve angle
τ	time constant
ψ	stall margin, see eq. (B13)
$\bar{\omega}$	pressure loss coefficient

Subscripts:

a	air
accel	acceleration
B	compressor bleed
B5	injection valve
b	burner
C	compressor
CB	cooling bleed
CD	compressor discharge
CV	control volume
cr	critical
decel	deceleration
dem	demand
err	error
F	fan

FD	fan discharge
FT	fan turbine
f	fuel
G	gas generator
g	governor
i	initial
in	into control volume
max	maximum value
min	minimum value
out	out of control volume
S	static
stall	value at stall
std	standard day
T	turbine
TD	turbine discharge
tot	total
v	butterfly valve
vf	fuel heating value
X	bleed system cross duct
0	design point value

APPENDIX B

SUMMARY OF EQUATIONS

This appendix contains all the equations that were used in the transient analysis of the YJ97/LF460 system. The equations are for the most part similar to previous practice in turbojet and turbofan engine dynamic analysis. Derivations of these equations may be found in references 12 and 13. The equation for calculating temperature under unsteady flow conditions is derived in appendix C. Component maps and fuel control parameters for the YJ97 turbojet were provided by the General Electric Company.

Figure 18 shows the flow of information that relates all the equations given in this appendix. The arrows indicate whether a particular variable is an input or an output for a given set of calculations. Through use of the information flow shown in figure 18, the YJ97/LF460 system was modeled as a set of simultaneous, ordinary differential equations.

YJ97 Compressor

$$\theta = \frac{T_2}{T_{std}} \quad (B1)$$

$$\delta = \frac{P_2}{P_{std}} \quad (B2)$$

$$\frac{\dot{w}_2 \sqrt{\theta}}{\delta} = \mathcal{F}_1 \left(\frac{P_3}{P_2}, \frac{N_G}{\sqrt{\theta}} \right) \quad (B3)$$

$$\eta_C = \mathcal{F}_2 \left(\frac{P_3}{P_2}, \frac{N_G}{\sqrt{\theta}} \right) \quad (B4)$$

Figure 19 shows the compressor map containing \mathcal{F}_1 and \mathcal{F}_2 .

$$T_{CD} = \frac{T_2 \left[\left(\frac{P_3}{P_2} \right)^{(\gamma_C - 1)/\gamma_C} - 1 \right]}{\eta_C} + T_2 \quad (B5)$$

$$\Delta h_C = C_{pC} (T_{CD} - T_2) \quad (B6)$$

$$\dot{w}_{CB} = \sqrt{\frac{\gamma_3 (\gamma_3 + 1)/(\gamma_3 - 1)}{R} \left(\frac{2}{\gamma_3 + 1} \right)} \frac{P_3 A_{CB}}{\sqrt{T_3}} \quad (B7)$$

$$w_3 = \int_0^t (\dot{w}_2 - \dot{w}_3 - \dot{w}_{CB} - \dot{w}_B) dt + w_{3,i} \quad (B8)$$

$$h_{CD} = a_1 T_{CD} + b_1 \quad (B9)$$

$$h_3 = a_1 T_3 + b_1 \quad (B10)$$

$$T_3 = \int_0^t \frac{1}{w_3} \left[\frac{\dot{w}_2 h_{CD} - (\dot{w}_3 + \dot{w}_{CB} + \dot{w}_B) h_3}{C_{V3}} - T_3 (\dot{w}_2 - \dot{w}_3 - \dot{w}_{CB} - \dot{w}_B) \right] dt + T_{3,i} \quad (B11)$$

$$P_3 = \frac{R w_3 T_3}{V_3} \quad (B12)$$

$$\psi = \left[\frac{\left(\frac{P_3}{P_2} \right)_{\text{stall}}}{\frac{P_3}{P_2}} \right] \left[\frac{\dot{w}_2 \sqrt{\theta/\delta}}{(\dot{w}_2 \sqrt{\theta/\delta})_{\text{stall}}} \right] - 1 \quad (B13)$$

YJ97 Combustor

$$\dot{w}_3 = \frac{A_3 g_c}{l_3} \int_0^t (P_3 - P_4 - C_{f3} \dot{w}_3^2) dt + \dot{w}_{3,i} \quad (\text{B14})$$

$$w_4 = \int_0^t (\dot{w}_3 + \dot{w}_f - \dot{w}_4) dt + w_{4,i} \quad (\text{B15})$$

$$h_{a4} = a_1 T_4 + b_1 \quad (\text{B16})$$

$$h_{f4} = a_2 T_4 + b_2 \quad (\text{B17})$$

$$h_4 = \frac{\dot{w}_3 h_{a4} + \dot{w}_f h_{f4}}{\dot{w}_3 + \dot{w}_f} \quad (\text{B18})$$

$$T_4 = \int_0^t \frac{1}{w_4} \left[\frac{\dot{w}_3 h_3 + \dot{w}_f h_{vf} \eta_b - \dot{w}_4 h_4}{C_{V4}} - T_4 (\dot{w}_3 + \dot{w}_f - \dot{w}_4) \right] dt + T_{4,i} \quad (\text{B19})$$

$$P_4 = \frac{R w_4 T_4}{V_4} \quad (\text{B20})$$

YJ97 Turbine

$$\frac{1000 \Delta h_T}{N_G \sqrt{T_4}} = \mathcal{F}_3 \left(\frac{P_{51}}{P_4}, \frac{N_G}{\sqrt{T_4}} \right) \quad (\text{B21})$$

$$\frac{\dot{w}_4 T_4}{N_G P_4} = \mathcal{F}_4 \left(\frac{P_{51}}{P_4}, \frac{N_G}{\sqrt{T_4}} \right) \quad (\text{B22})$$

Figure 20 shows the form of the turbine maps \mathcal{F}_3 and \mathcal{F}_4

$$T_{TD} = T_4 - \frac{\Delta h_T}{C_{pT}} \quad (B23)$$

$$h_{TD} = a_3 T_{TD} + b_3 \quad (B24)$$

$$T_5 = \frac{1}{a_3} \left(\frac{\dot{w}_4 h_{TD} + \dot{w}_{CB} h_3}{\dot{w}_5} - b_3 \right) \quad (B25)$$

$$\dot{w}_5 = \dot{w}_4 + \dot{w}_{CB} \quad (B26)$$

$$h_5 = a_3 T_5 + b_3 \quad (B27)$$

YJ97 Rotor

$$L_C = \frac{K_L \Delta h_c \dot{w}_2}{N_G} \quad (B28)$$

$$L_T = \frac{K_L \Delta h_T \dot{w}_4}{N_G} \quad (B29)$$

$$N_G = \frac{K_N}{I_G} \int_0^t (L_T - L_C) dt + N_{G,i} \quad (B30)$$

YJ97 Fuel Control

$$\dot{w}_{fg} = \dot{w}_{f,i} + \Delta \dot{w}_f \quad (B31)$$

$$N_{err} = N_{dem} - N_G \quad (B32)$$

The main governor loop was simulated by a transfer function:

$$\frac{\Delta \dot{w}_f(s)}{N_{err}(s)} = \frac{K_1(\tau_1 s + 1)}{s(\tau_2 s + 1)(\tau_3 s + 1)} \quad (B33)$$

$$\left(\frac{\dot{w}_f}{P_{3S}}\right)_{\text{accel}} = \mathcal{F}_5(N_G, T_2) \quad (\text{B34})$$

Figure 21 shows the form of the acceleration schedule \mathcal{F}_5 .

$$\dot{w}_{f, \text{accel}} = 0.946 P_3 \left(\frac{\dot{w}_f}{P_{3S}}\right)_{\text{accel}} \quad (\text{B35})$$

$$\dot{w}_{f, \text{decel}} = \frac{\dot{w}_{f, \text{accel}}}{3} \quad (\text{B36})$$

The coefficient 0.946 is used to obtain static pressure, P_{3S} , from total pressure, P_3 .

$$\dot{w}_{f1} = \min \left\{ \begin{array}{l} \dot{w}_{fg} \\ \dot{w}_{f, \text{accel}} \end{array} \right\} \quad (\text{B37})$$

$$\dot{w}_f = \max \left\{ \begin{array}{l} \dot{w}_{f1} \\ \dot{w}_{f, \text{decel}} \end{array} \right\} \quad (\text{B38})$$

Exhaust Duct (Bleed System Only)

$$w_{51} = \int_0^t (\dot{w}_5 + \dot{w}_{B5} - \dot{w}_{54}) dt + w_{51, i} \quad (\text{B39})$$

$$T_{51} = \int_0^t \frac{1}{w_{51}} \left[\frac{\dot{w}_5 h_5 + \dot{w}_{B5} h_X - \dot{w}_{54} h_{51}}{C_{V51}} - T_{51} (\dot{w}_5 + \dot{w}_{B5} - \dot{w}_{54}) \right] dt + T_{51, i} \quad (\text{B40})$$

$$P_{51} = \frac{R w_{51} T_{51}}{V_{51}} \quad (\text{B41})$$

$$P_{54} = 0.89 P_{51} \quad (\text{B42})$$

$$h_{51} = a_3 T_{51} + b_3 \quad (\text{B43})$$

Exhaust Duct and Valves (ETC System Only)

$$w_{51} = \int_0^t (\dot{w}_5 + \dot{w}_{5X} - \dot{w}_{52}) dt + w_{51,i} \quad (\text{B44})$$

$$h_{51} = a_3 T_{51} + b_3 \quad (\text{B45})$$

$$T_{51} = \int_0^t \frac{1}{w_{51}} \left[\frac{\dot{w}_5 h_5 + \dot{w}_{5X} h_{5X} - \dot{w}_{52} h_{51}}{C_{V51}} - T_{51} (\dot{w}_5 + \dot{w}_{5X} - \dot{w}_{52}) \right] dt + T_{51,i} \quad (\text{B46})$$

$$P_{51} = \frac{R w_{51} T_{51}}{V_{51}} \quad (\text{B47})$$

$$P_{52} = 0.95 P_{51} \quad (\text{B48})$$

$$\Delta P_v = q_{52} \bar{\omega}_v \quad (\text{B49})$$

$$q_{52} = \frac{(\dot{w}_{52})^2 R T_{51}}{2 P_{52} (A_{52})^2} \quad (\text{B50})$$

$$\bar{\omega}_v = \mathcal{F}_6(\theta_v) \quad (\text{B51})$$

Figure 22 shows \mathcal{F}_6 , the butterfly valve loss coefficient, as a function of valve angle (ref. 6)

$$\dot{w}_{52} = \frac{A_{52} g_c}{l_{52}} \int_0^t (P_{52} - P_{53} - \Delta P_v) dt + \dot{w}_{52,i} \quad (\text{B52})$$

$$w_{53} = \int_0^t (\dot{w}_{52} - \dot{w}_{54}) dt + w_{53,i} \quad (\text{B53})$$

$$h_{53} = a_3 T_{53} + b_3 \quad (\text{B54})$$

$$T_{53} = \int_0^t \frac{1}{w_{53}} \left[\frac{\dot{w}_{52} h_{51} - \dot{w}_{54} h_{53}}{C_{V53}} - T_{53} (\dot{w}_{52} - \dot{w}_{54}) \right] dt + T_{53,i} \quad (\text{B55})$$

$$P_{53} = \frac{R w_{53} T_{53}}{V_{53}} \quad (\text{B56})$$

$$P_{54} = 0.9635 P_{53} \quad (\text{B57})$$

Cross Duct and Valves (Bleed System Only)

The isentropic nozzle equations were used in treating the bleed and injection valves as variable-area orifices. The Mach number downstream of the valves was assumed to be low, so that downstream static and total pressures could be assumed equal.

Bleed Valves

$$P_{X, cr} = P_3 \left(\frac{2}{\gamma_3 + 1} \right)^{\gamma_3 / (\gamma_3 - 1)} \quad (\text{B58})$$

If $P_X \geq P_{X, cr}$, equation (B59) applies:

$$\dot{w}_B = P_3 \sqrt{\frac{g_c}{RT_3}} A_B \left(\frac{P_X}{P_3} \right)^{1/\gamma_3} \sqrt{\left(\frac{2\gamma_3}{\gamma_3 - 1} \right) \left[1 - \left(\frac{P_X}{P_3} \right)^{(\gamma_3 - 1)/\gamma_3} \right]} \quad (\text{B59})$$

If $P_X < P_{X, cr}$, equation (B60) applies:

$$\dot{w}_B = \sqrt{\frac{\gamma_3}{R} \left(\frac{2}{\gamma_3 + 1} \right)^{(\gamma_3+1)/(\gamma_3-1)} \frac{P_3 A_B}{\sqrt{T_3}}} \quad (\text{B60})$$

Injection Valves

$$P_{51, cr} = P_X \left(\frac{2}{\gamma_X + 1} \right)^{\gamma_X/(\gamma_X-1)} \quad (\text{B61})$$

If $P_{51} \geq P_{51, cr}$, equation (B62) applies:

$$\dot{w}_{B5} = P_X \sqrt{\frac{g_c}{RT_X}} A_X \left(\frac{P_{51}}{P_X} \right)^{1/\gamma_X} \sqrt{\left(\frac{2\gamma_X}{\gamma_X - 1} \right) \left[1 - \left(\frac{P_{51}}{P_X} \right)^{(\gamma_X-1)/\gamma_X} \right]} \quad (\text{B62})$$

If $P_{51} < P_{51, cr}$, equation (B63) applies:

$$\dot{w}_{B5} = \sqrt{\frac{\gamma_X}{R} \left(\frac{2}{\gamma_X + 1} \right)^{(\gamma_X+1)/(\gamma_X-1)} \frac{P_X A_X}{\sqrt{T_X}}} \quad (\text{B63})$$

$$w_X = \int_0^t (\dot{w}_{BI} + \dot{w}_{BII} - \dot{w}_{B5I} - \dot{w}_{B5II}) dt + w_{X, i} \quad (\text{B64})$$

$$T_X = \int_0^t \frac{1}{w_X}$$

$$\left[\frac{\dot{w}_{BI} h_{BI} + \dot{w}_{BII} h_{BII} - \dot{w}_{B5I} h_X - \dot{w}_{B5II} h_X}{C_{VX}} - T_X (\dot{w}_{BI} + \dot{w}_{BII} - \dot{w}_{B5I} - \dot{w}_{B5II}) \right] dt + T_{X, i} \quad (\text{B65})$$

$$P_X = \frac{R w_X T_X}{V_X} \quad (\text{B66})$$

$$h_X = a_1 T_X + b_1 \quad (B67)$$

Cross Duct (ETC System Only)

$$\dot{w}_{5X} = \frac{A_{5X} g_c}{\left(\frac{l_{5X}}{2}\right)} \int_0^t (P_{5X} - P_{51} - C_{f5X} \dot{w}_{5X}^2) dt + \dot{w}_{5X,i} \quad (B68)$$

$$w_{5X} = \int_0^t (-\dot{w}_{5XI} - \dot{w}_{5XII}) dt + w_{5X,i} \quad (B69)$$

$$h_{5X} = a_3 T_{5X} + b_3 \quad (B70)$$

$$T_{5X} = \int_0^t \frac{1}{w_{5X}} \left[\frac{-h_{5X}(\dot{w}_{5XI} + \dot{w}_{5XII})}{C_{VX}} + T_{5X}(\dot{w}_{5XI} + \dot{w}_{5XII}) \right] dt + T_{5X,i} \quad (B71)$$

$$P_{5X} = \frac{R w_{5X} T_{5X}}{V_{5X}} \quad (B72)$$

LF460 Turbine

$$P_{55S, cr} = P_{54} \left(\frac{2}{\gamma_{54} + 1} \right)^{\gamma_{54}/(\gamma_{54}-1)} \quad (B73)$$

If $P_{55S} \geq P_{55S, cr}$, equation (B74) applies:

$$\dot{w}_{54} = P_{54} \sqrt{\frac{g_c}{RT_{54}}} A_{54} \left(\frac{P_{55S}}{P_{54}} \right)^{1/\gamma_{54}} \sqrt{\left(\frac{2\gamma_{54}}{\gamma_{54} - 1} \right) \left[1 - \left(\frac{P_{55S}}{P_{54}} \right)^{(\gamma_{54}-1)/\gamma_{54}} \right]} \quad (B74)$$

If $P_{55S} < P_{55S, cr}$, equation (B75) applies:

$$\dot{w}_{54} = \sqrt{\frac{\gamma_{54}}{R} \left(\frac{2}{\gamma_{54} + 1} \right)^{(\gamma_{54}+1)/(\gamma_{54}-1)} \frac{P_{54} A_{54}}{\sqrt{T_{54}}}} \quad (\text{B75})$$

$$\frac{\Delta h_{\text{FT}}}{C_{p\text{FT}} T_{54}} = \mathcal{F}_7 \left(\frac{N_{\text{F}}}{\sqrt{T_{54}}}, \frac{P_{54}}{P_{55\text{S}}} \right) \quad (\text{B76})$$

$$\eta_{\text{FT}} = \mathcal{F}_8 \left(\frac{N_{\text{F}}}{\sqrt{T_{54}}}, \frac{P_{54}}{P_{55\text{S}}} \right) \quad (\text{B77})$$

Figure 23 shows the LF460 turbine map containing \mathcal{F}_7 and \mathcal{F}_8 .

$$T_{55} = T_{54} \left(1 - \frac{\Delta h_{\text{FT}}}{C_{p\text{FT}} T_{54}} \right) \quad (\text{B78})$$

$$P_{55} = P_{54} \left(1 - \frac{T_{54} - T_{55}}{\eta_{\text{FT}} T_{54}} \right)^{\gamma_{\text{FT}}/(\gamma_{\text{FT}}-1)} \quad (\text{B79})$$

LF460 Fan

$$\frac{\dot{w}_{22} \sqrt{\theta}}{\delta} = \mathcal{F}_9 \left(\frac{N_{\text{F}}}{\sqrt{\theta}}, \frac{P_{23}}{P_2} \right) \quad (\text{B80})$$

$$\eta_{\text{F}} = \mathcal{F}_{10} \left(\frac{N_{\text{F}}}{\sqrt{\theta}}, \frac{P_{23}}{P_2} \right) \quad (\text{B81})$$

Figure 24 shows the LF460 fan maps \mathcal{F}_9 and \mathcal{F}_{10} .

$$T_{\text{FD}} = \frac{T_2 \left[\left(\frac{P_{23}}{P_2} \right)^{(\gamma_{\text{F}}-1)/\gamma_{\text{F}}} - 1 \right]}{\eta_{\text{F}}} + T_2 \quad (\text{B82})$$

$$w_{23} = \int_0^t (\dot{w}_{22} - \dot{w}_{28})dt + w_{23,i} \quad (\text{B83})$$

$$h_{FD} = a_1 T_{FD} + b_1 \quad (\text{B84})$$

$$h_{23} = a_1 T_{23} + b_1 \quad (\text{B85})$$

$$T_{23} = \int_0^t \frac{1}{w_{23}} \left[\frac{\dot{w}_{23} h_{FD} - \dot{w}_{28} h_{23}}{C_{V23}} - T_{23} (\dot{w}_{23} - \dot{w}_{28}) \right] dt + T_{23,i} \quad (\text{B86})$$

$$P_{23} = \frac{R w_{23} T_{23}}{V_{23}} \quad (\text{B87})$$

LF460 Exhaust and Spoilers

A fan installation was assumed in which the turbine and fan discharge streams were unmixed. However, the spoilers had an effect on both discharge streams.

$$C_{VL28} = \mathcal{F}_{11}(\beta) \quad (\text{B88})$$

$$C_{VL8} = \mathcal{F}_{11}(\beta) \quad (\text{B89})$$

$$C_{w28} = \mathcal{F}_{12}(\beta) \quad (\text{B90})$$

$$C_{w8} = \mathcal{F}_{13}(\beta) \quad (\text{B91})$$

The functions \mathcal{F}_{11} , \mathcal{F}_{12} , and \mathcal{F}_{13} (velocity and flow coefficient as a function of spoiler angle) are shown in figures 25 to 27. These figures are based on data provided by the General Electric Company.

$$P_7 = 0.98 P_{55} \quad (\text{B92})$$

$$\dot{w}_8 = P_7 \sqrt{\frac{g_c}{RT_{55}}} C_{w8} A_8 \left(\frac{P_2}{P_7}\right)^{1/\gamma_{55}} \sqrt{\left(\frac{2\gamma_{55}}{\gamma_{55} - 1}\right) \left[1 - \left(\frac{P_2}{P_7}\right)^{(\gamma_{55}-1)/\gamma_{55}}\right]} \quad (\text{B93})$$

$$F_8 = C_{VL8} \sqrt{\frac{2J}{g_c}} \dot{w}_8 \sqrt{C_{p55} T_{55} \left[1 - \left(\frac{P_2}{P_7}\right)^{(\gamma_{55}-1)/\gamma_{55}}\right]} \quad (\text{B94})$$

$$P_{27} = 0.99 P_{23} \quad (\text{B95})$$

$$\dot{w}_{28} = P_{27} \sqrt{\frac{g_c}{RT_{23}}} C_{w28} A_{28} \left(\frac{P_2}{P_{27}}\right)^{1/\gamma_{23}} \sqrt{\left(\frac{2\gamma_{23}}{\gamma_{23} - 1}\right) \left[1 - \left(\frac{P_2}{P_{27}}\right)^{(\gamma_{23}-1)/\gamma_{23}}\right]} \quad (\text{B96})$$

$$F_{28} = C_{VL28} \sqrt{\frac{2J}{g_c}} \dot{w}_{28} \sqrt{C_{p23} T_{23} \left[1 - \left(\frac{P_2}{P_{23}}\right)^{(\gamma_{23}-1)/\gamma_{23}}\right]} \quad (\text{B97})$$

$$F_{\text{tot}} = 0.96(F_8 + F_{28}) \quad (\text{B98})$$

The factor of 0.96 is a correction for base drag.

LF460 Rotor

$$L_F = \frac{K_L C_{pF} (T_{FD} - T_2) \dot{w}_{22}}{N_F} \quad (\text{B99})$$

$$L_{FT} = \frac{K_L C_{pFT} T_{54} \left(\frac{\Delta h_{FT}}{C_{pFT} T_{54}}\right) \dot{w}_{54}}{N_F} \quad (\text{B100})$$

$$N_F = \frac{K_N}{I_F} \int_0^t (L_{FT} - L_F) dt + N_{F,i} \quad (\text{B101})$$

Actuators

$$\theta_v = 20 \int_0^t (\theta_{v,dem} - \theta_v) dt + \theta_{v,i} \quad (\text{B102})$$

$$\beta = 20 \int_0^t (\beta_{dem} - \beta) dt + \beta_i \quad (\text{B103})$$

$$A_B = 20 \int_0^t (A_{B,dem} - A_B) dt + A_{B,i} \quad (\text{B104})$$

$$A_X = 20 \int_0^t (A_{X,dem} - A_X) dt + A_{X,i} \quad (\text{B105})$$

$$A_{XI,dem} = 2A_{BII,dem} \quad (\text{B106})$$

$$A_{XII,dem} = 2A_{BI,dem} \quad (\text{B107})$$

APPENDIX C

DERIVATION OF TEMPERATURE EQUATION

Defining total internal energy as

$$e = e_S + \frac{u^2}{2} \quad (C1)$$

and total enthalpy as

$$h = h_S + \frac{u^2}{2} \quad (C2)$$

the first law of thermodynamics for unsteady flow through a control volume (ref. 12) becomes

$$\frac{d}{dt} (w_{CV} e_{CV}) = \sum \dot{w}_{in} h_{in} - \sum \dot{w}_{out} h_{out} \quad (C3)$$

$$\dot{w}_{CV} e_{CV} + w_{CV} \dot{e}_{CV} = \sum \dot{w}_{in} h_{in} - \sum \dot{w}_{out} h_{out} \quad (C4)$$

Considering the control volume as a lumped element

$$\dot{w}_{CV} = \sum \dot{w}_{in} - \sum \dot{w}_{out} \quad (C5)$$

$$T_{out} = T_{CV} \quad (C6)$$

$$h_{out} = h(T_{CV}) = h_{CV} \quad (C7)$$

where T_{CV} is the total temperature in the control volume.

With the preceding assumptions, equation (C4) becomes

$$e_{CV} = \frac{\sum \dot{w}_{in} h_{in} - \sum \dot{w}_{out} h_{CV} - e_{CV} \left(\sum \dot{w}_{in} - \sum \dot{w}_{out} \right)}{w_{CV}} \quad (C8)$$

Finally, assuming $e = C_V T$, equation (C8) becomes

$$C_V \dot{T}_{CV} = \frac{\sum \dot{w}_{in} h_{in} - \sum \dot{w}_{out} h_{CV} - C_V T_{CV} (\sum \dot{w}_{in} - \sum \dot{w}_{out})}{w_{CV}} \quad (C9)$$

$$\dot{T}_{CV} = \int_0^t \frac{1}{w_{CV}} \left[\frac{\sum \dot{w}_{in} h_{in} - \sum \dot{w}_{out} h_{CV}}{C_V} - T_{CV} (\sum \dot{w}_{in} - \sum \dot{w}_{out}) \right] dt + T_{CV,i} \quad (C10)$$

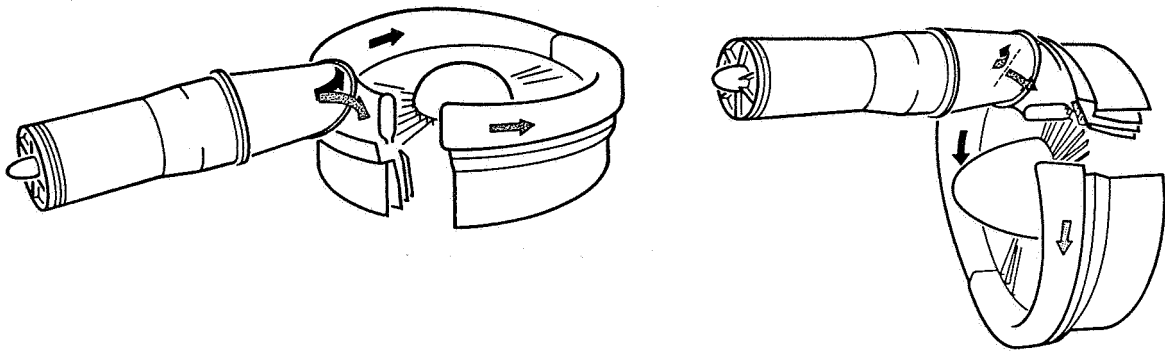
REFERENCES

1. Anon.: Near Term V/STOL Lift Fan Research Transport Update. Vol. I - Technical Data. Rep. MDC A1602, McDonnell Aircraft Co., July 1972. (Contract NAS2-5499.)
2. Anon.: Design Study of V/STOL Lift Fan Research Transport. Final Report, Vol. I, Pt. I, Task II. Rep. D6-22523, The Boeing Co., 1972. (Contract NAS2-6563.)
3. Anon.: Study of Near-Term V/STOL Lift-Fan Research Transport. Vol. I. Rep. NA-72-444, North American Rockwell Corp., 1972. (Contract NAS2-6564.)
4. Smith, Eugene G.: Investigations of a Variable Area Scroll for Power Transfer in Tip Turbine Lift Fan Systems. Rep. 67FPD218, General Electric Co., (USAAVLABS TR-67-26, AD-667989), Nov. 1967.
5. Anon.: Advanced Lift Fan V/STOL Aircraft System Study. Vol. I. Rep. MDC A0513, McDonnell Aircraft Co., June 1970. (Contract NAS2-5499.)
6. Anon.: A Full Scale Test of a New V/STOL Control System: Energy Transfer Control (ETC). Rep. MDC A1588, McDonnell Aircraft Co., June 1972. (Contract NAS2-5499.)
7. Sellers, James F.: Steady State Analysis of Energy Transfer Control (ETC) and Compressor Bleed Concepts of Remote Lift Fan Control. NASA TM X-2876, 1973.
8. Anon.: Model Specification E-1155, Engine, Aircraft, Turbojet, YJ97-GE-100. General Electric Co., Cincinnati, Ohio, Oct. 1969.
9. Anon.: LF460 Detail Design. Rep. 71-AEG-297, General Electric Co. (NASA CR-120787), Sept. 1971.
10. Anon.: V/STOL Handling Qualities Criteria. 1: Criteria and Discussion. Rep. R-577-70, AGARD, Dec. 1970.
11. Sellers, J. F.; and Szuch, J. R.: Control of Turbofan Lift Engines for VTOL Aircraft. NASA TM X-68175, 1973.
12. Shapiro, Ascher H.: The Dynamics and Thermodynamics of Compressible Fluid Flow. Vol. I. Ronald Press Co., 1953.
13. Seldner, Kurt; Mihalow, James R.; and Blaha, Ronald J.: Generalized Simulation Technique for Turbojet Engine System Analysis. NASA TN D-6610, 1972.

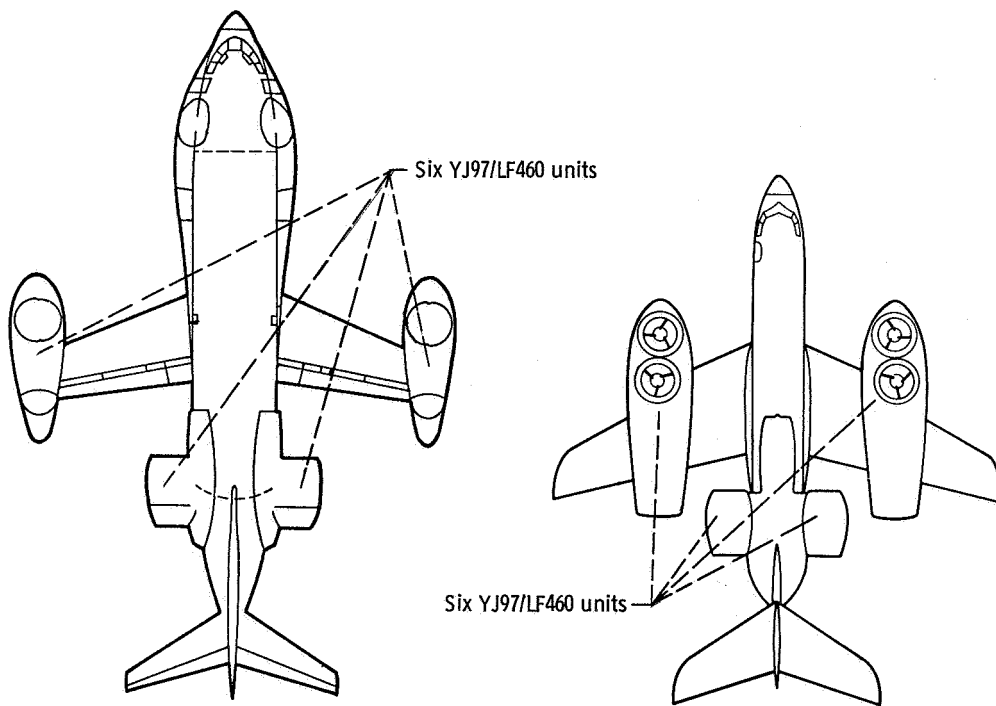
TABLE I. - YJ97/LF460 DESIGN -POINT PERFORMANCE

[Sea-level standard-day conditions; YJ97 military rating.]

YJ97 gas generator	
Compressor inlet pressure, P_{20} , kN/m^2 ; psia	101.4; 14.70
Compressor inlet temperature, T_{20} , K; $^{\circ}\text{R}$	288.2; 518.7
Exhaust gas temperature (EGT), T_{50} , K; $^{\circ}\text{R}$	1019; 1835
Exhaust gas pressure, P_{50} , kN/m^2 ; psia	365.2; 52.96
Exhaust gas flow rate, \dot{w}_{50} , kg/sec; lbm/sec	32.00; 70.54
Fuel flow rate, \dot{w}_{f0} , kg/sec; lbm/sec	0.6074; 1.339
Rotor speed (101.5 percent of design), N_{G0} , rad/sec; rpm	1451; 13 855
LF460 fan	
Fan inlet pressure, P_{220} , kN/m^2 ; psi	101.4; 14.70
Fan inlet temperature, T_{220} , K; $^{\circ}\text{R}$	288.2; 518.7
Turbine inlet temperature, T_{220} , K; $^{\circ}\text{R}$	1019; 1835
Turbine inlet pressure, P_{540} , kN/m^2 ; psia	325.0; 47.13
Turbine inlet flow rate, \dot{w}_{540} , kg/sec; lbm/sec	32.00; 70.54
Total thrust, F_0 , N; lbf	56 850; 12 780
Rotor speed (92.26 percent of design), N_{F0} , rad/sec; rpm	415.4; 3967



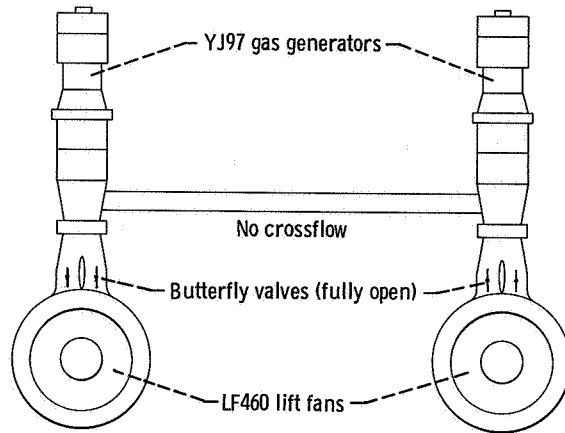
(a) Uninstalled.



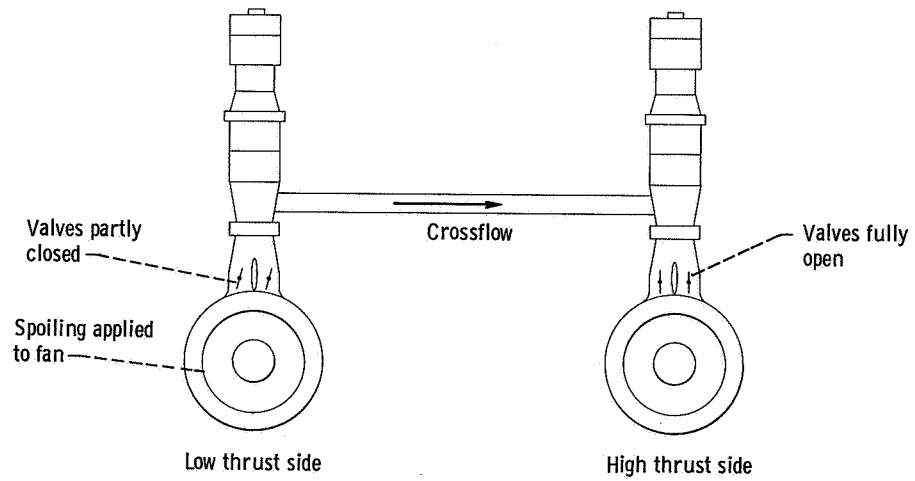
(b) Two aircraft concepts.

CD-11501-02

Figure 1. - YJ97/L460 configurations.

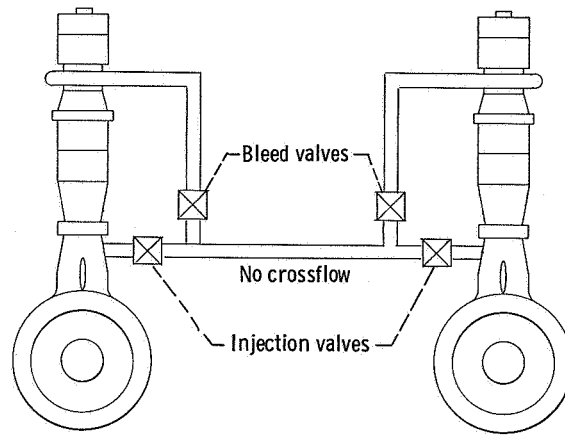


(a) Trim condition.

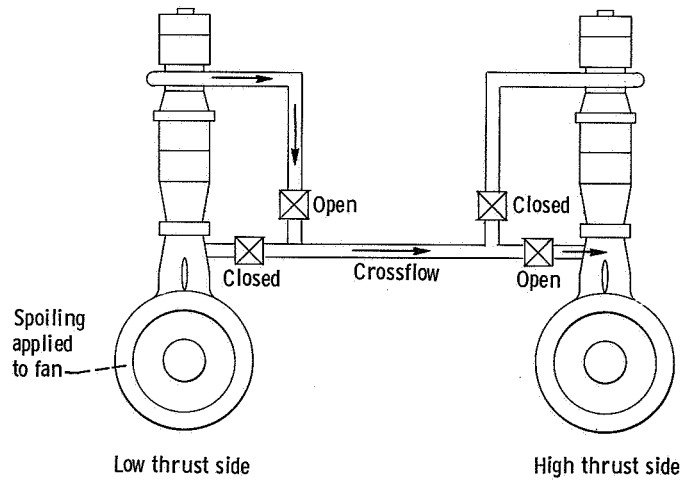


(b) Moment condition.

Figure 2. - Energy transfer control (ETC) system.

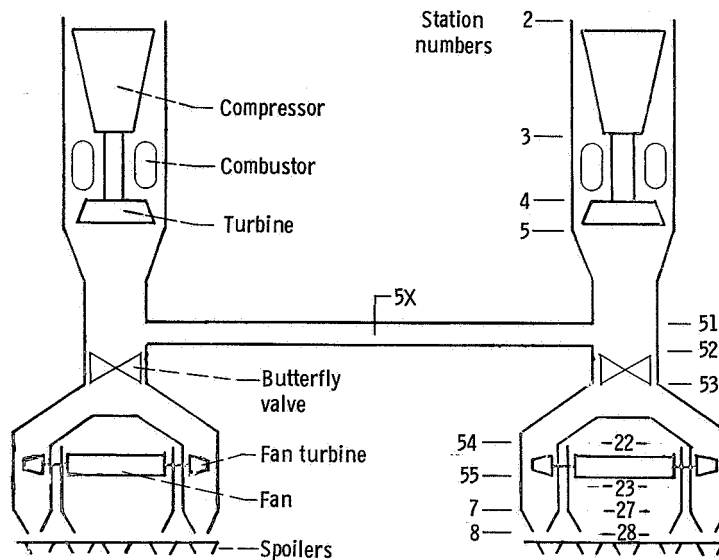


(a) Trim condition. All valves closed.

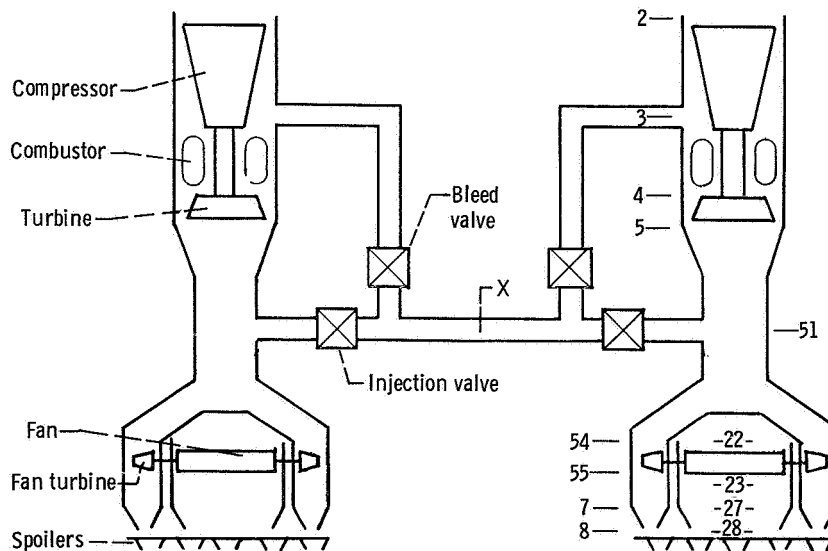


(b) Moment condition.

Figure 3. - Compressor bleed system.

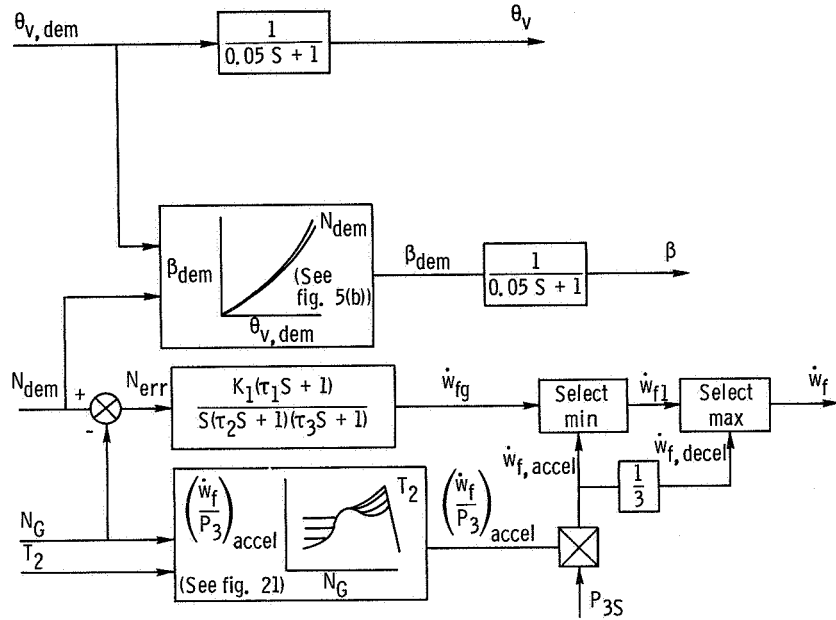


(a) ETC system.

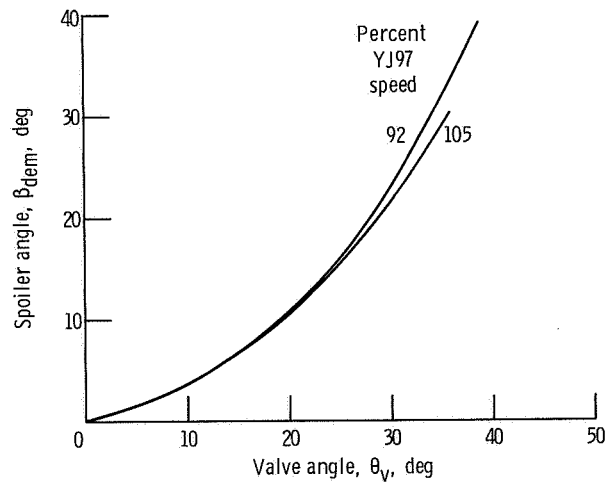


(b) Compressor bleed system.

Figure 4. - Component schematic.

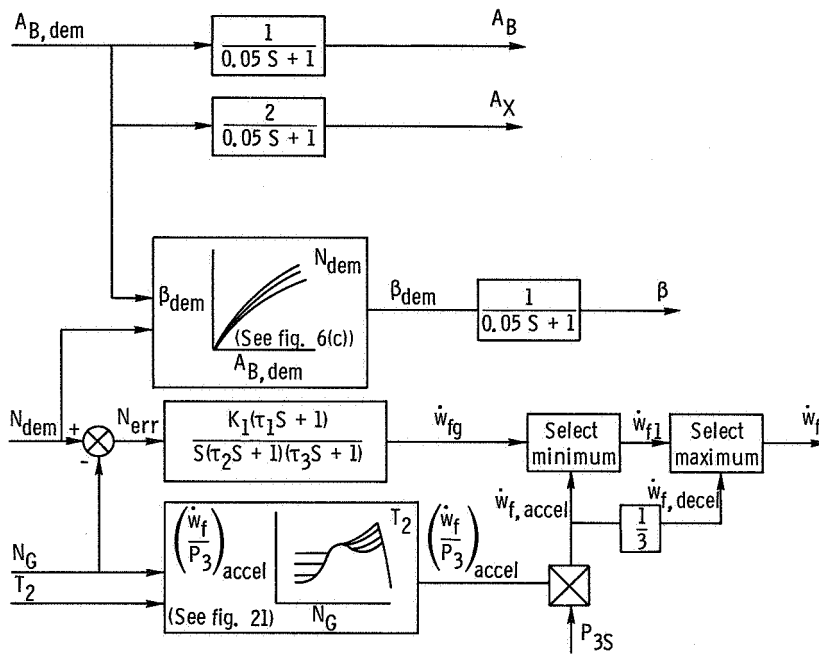


(a) Overall schematic.

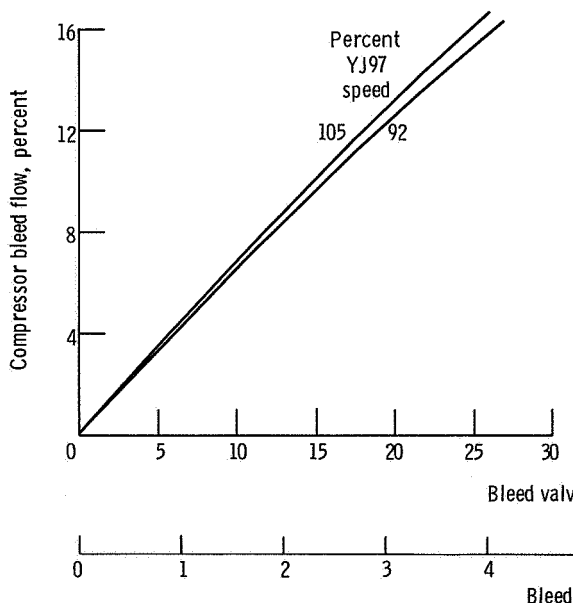


(b) Spoiler schedule.

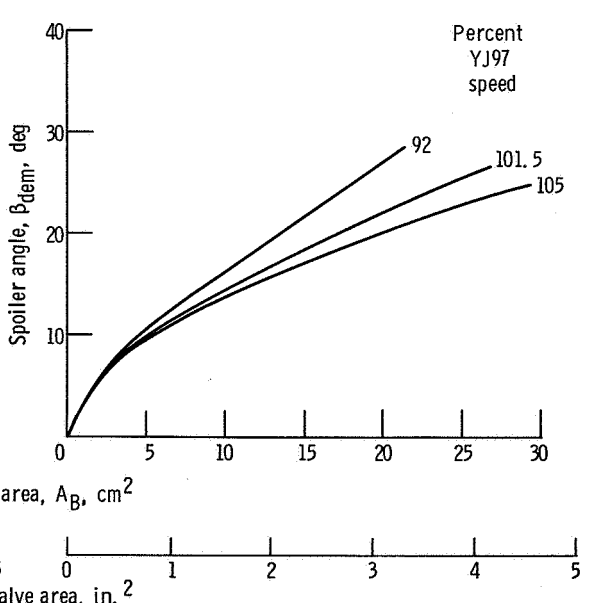
Figure 5. - ETC system controls.



(a) Overall schematic.



(b) Bleed flow as function of valve area.



(c) Spoiler schedule.

Figure 6. - Compressor bleed system controls.

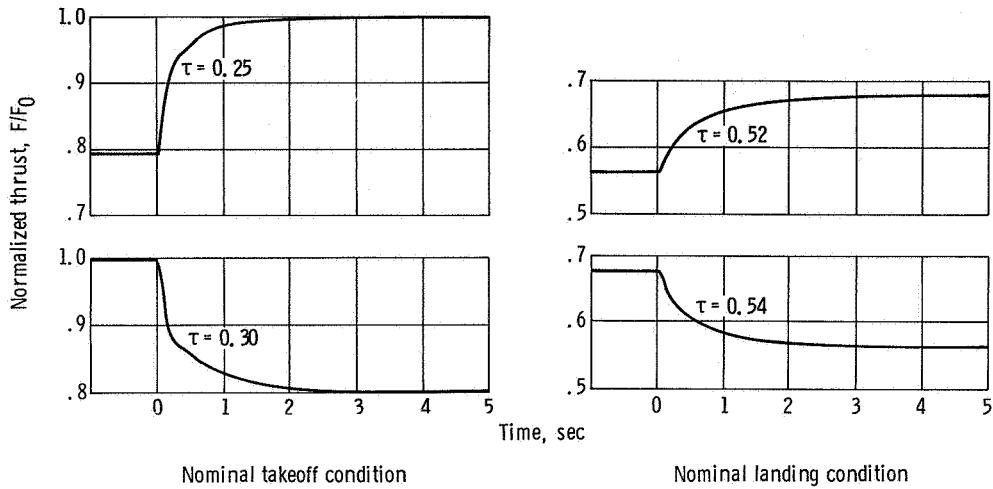


Figure 7. - YJ97/LF460 collective lift response (both systems).

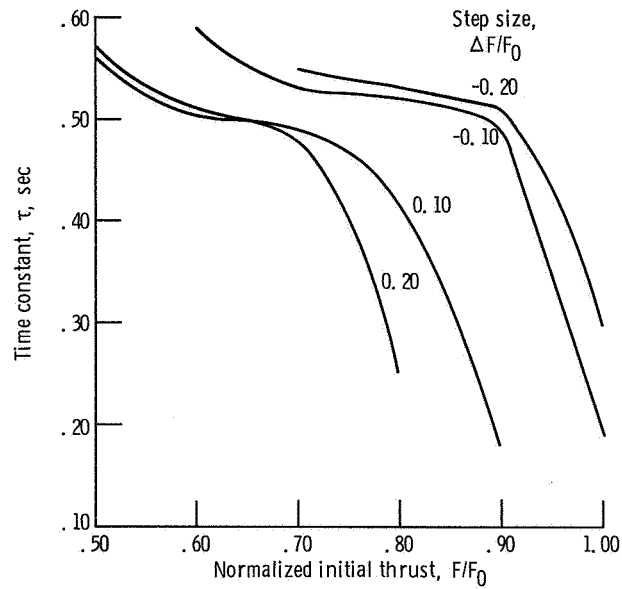
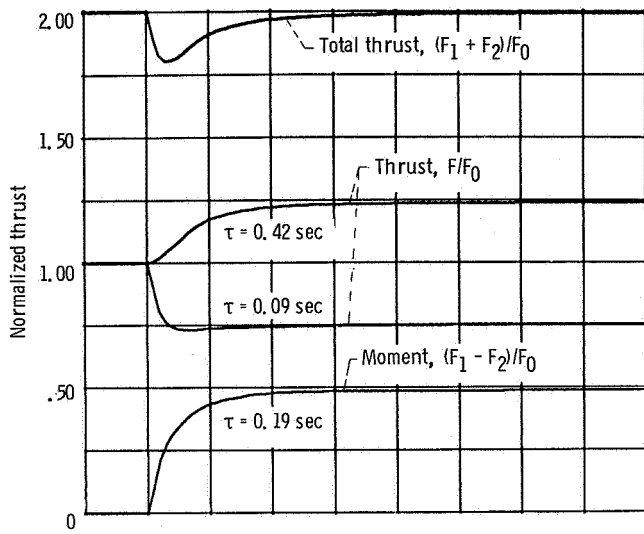
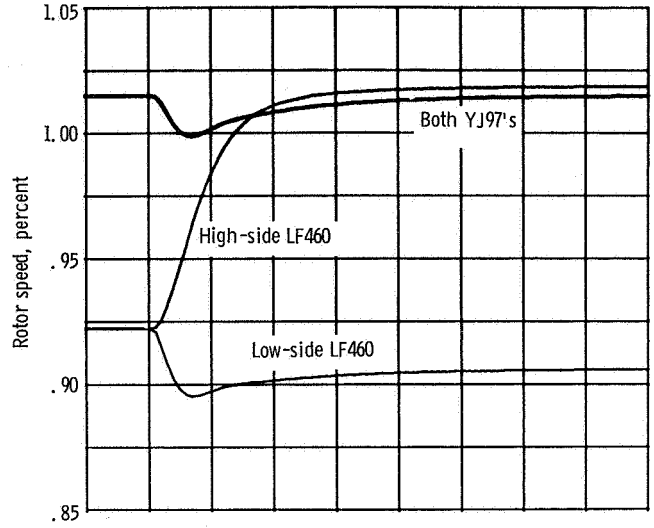


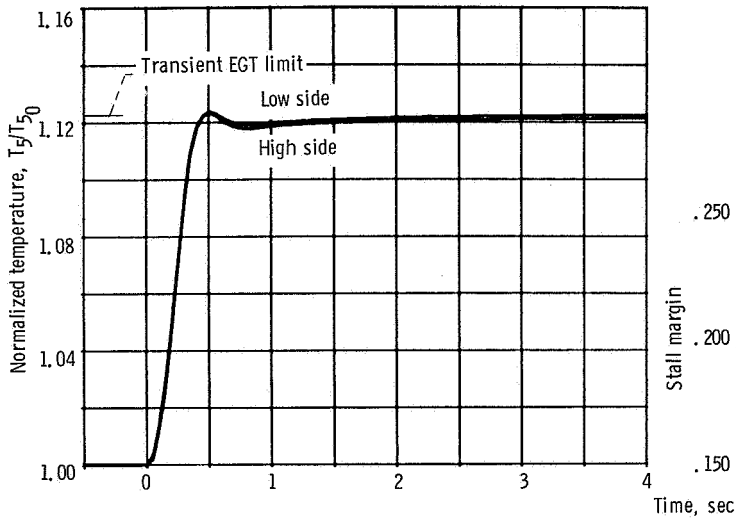
Figure 8. - Variation of lift response time constant with initial thrust level.



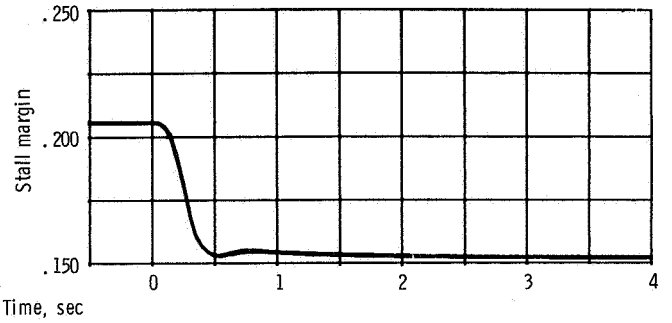
(a) Normalized thrust and moment.



(b) Rotor speed.

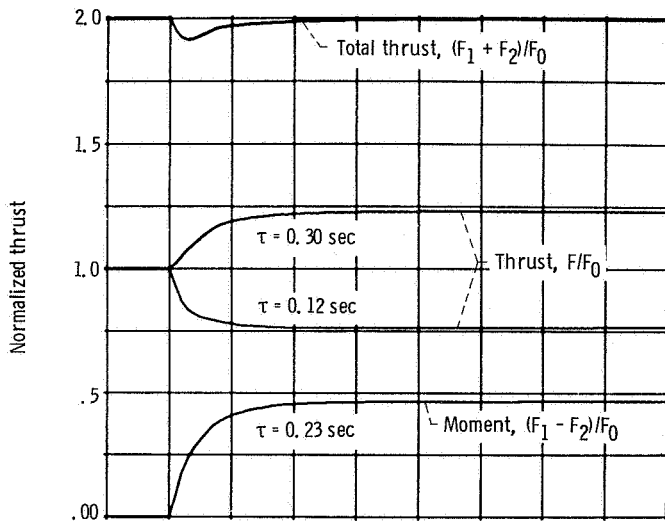


(c) YJ97 exhaust gas temperature.

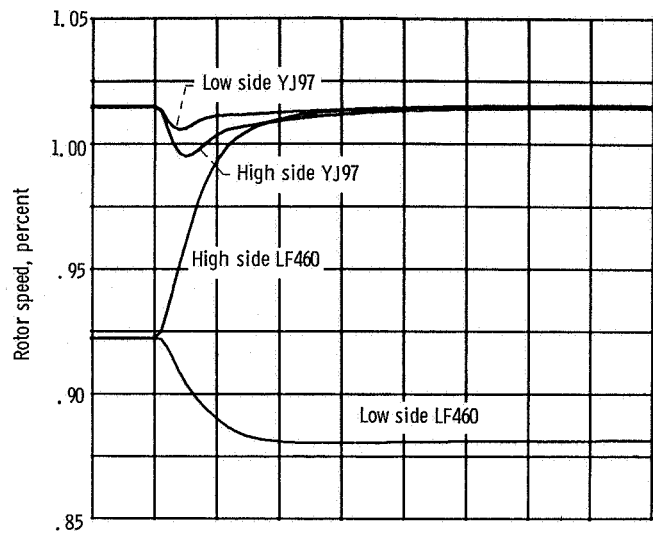


(d) YJ97 compressor stall margin. High and low sides indistinguishable.

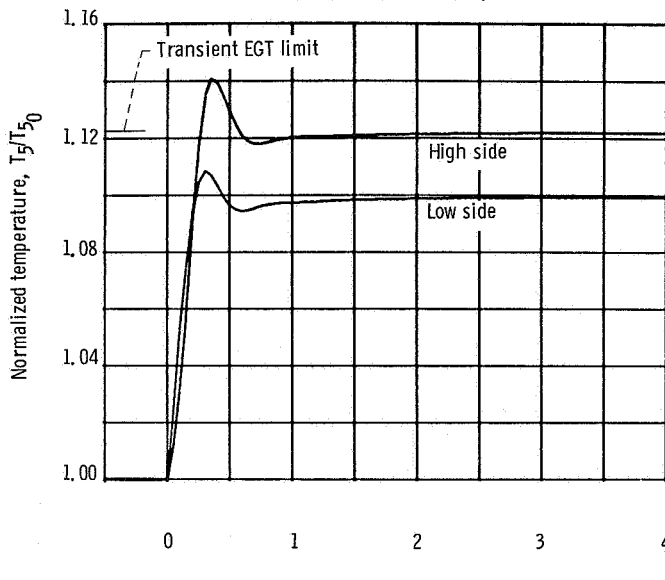
Figure 9. - ETC system response to 33.5° step in valve position; 101.5 percent YJ97 speed.



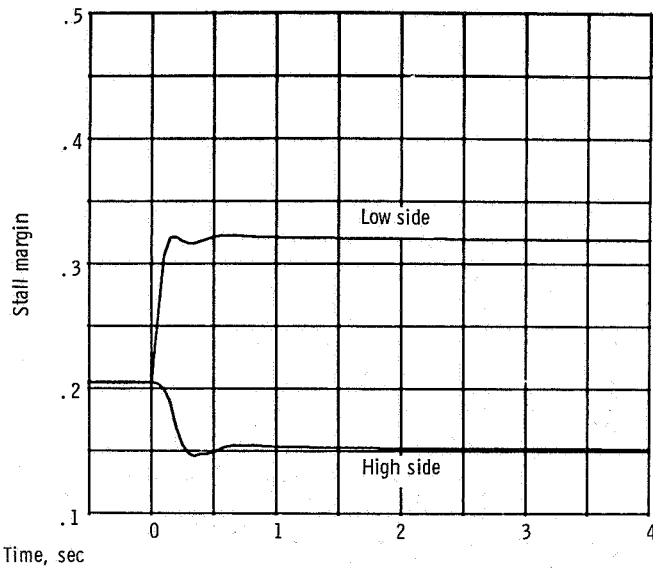
(a) Thrust and moment.



(b) Rotor speed.



(c) YJ97 exhaust gas temperature.



(d) YJ97 compressor stall margin.

Figure 10. - Bleed system response to 19.1-square-centimeter (2.95-in.²) step in bleed valve area; 101.5 percent YJ97 speed.

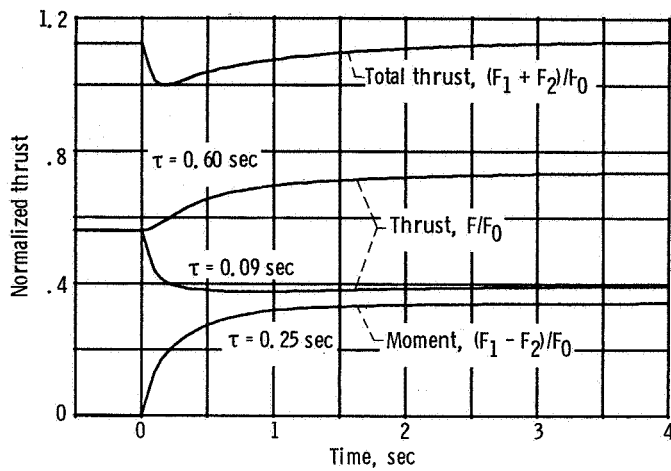


Figure 11. - ETC system response to 33.5° step in valve position; 92 percent YJ97 speed.

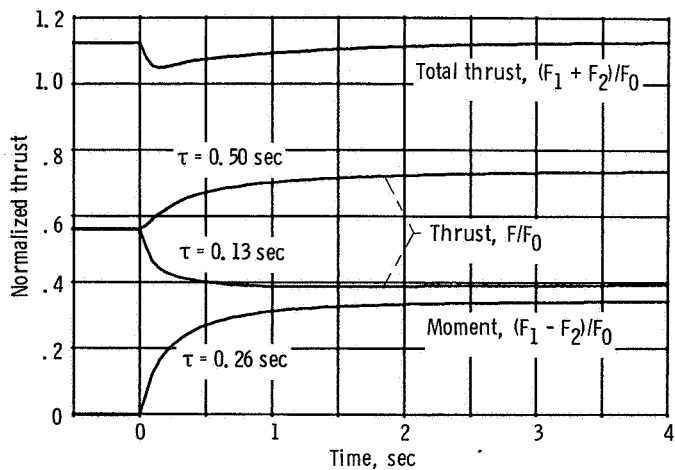


Figure 12. - Bleed system response to 19.1-square-centimeter (2.95-in.²) step in bleed valve area; 92 percent YJ97 speed.

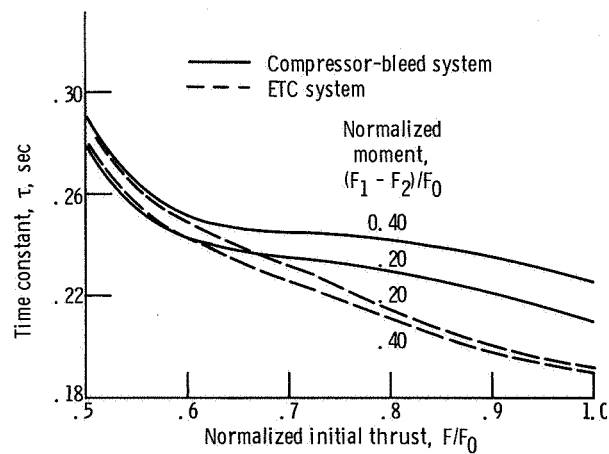


Figure 13. - Variation of moment time constant with initial thrust level.

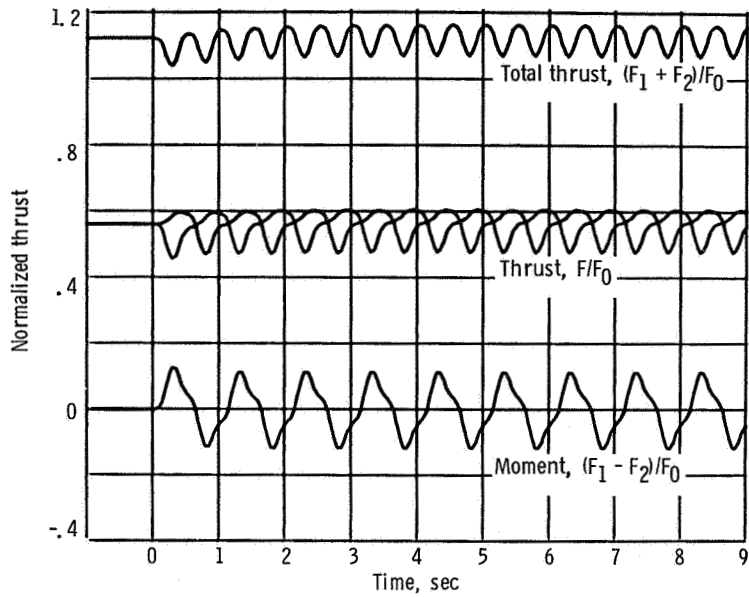


Figure 14. - Response of ETC system to 1-hertz sinusoidal valve inputs. Peak valve deflection, 30° ; 92 percent YJ97 speed.

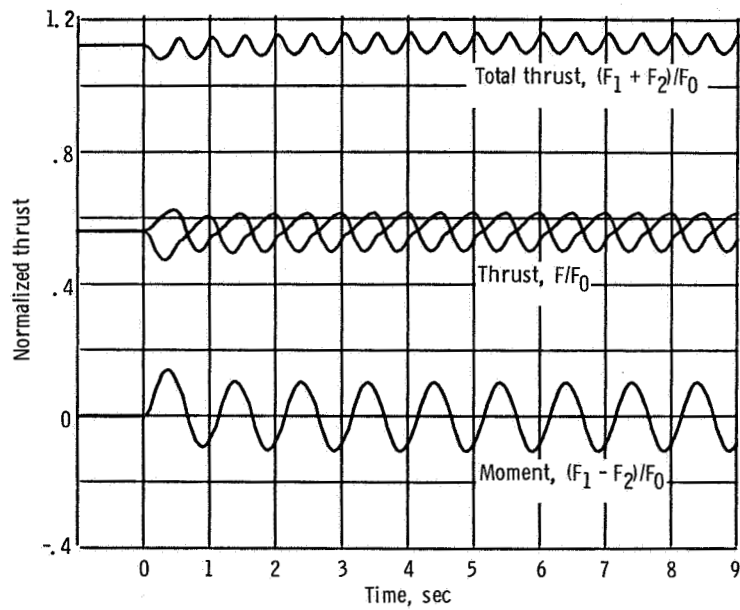


Figure 15. - Response of bleed system to 1-hertz sinusoidal valve inputs. Peak bleed valve area, 12.9 square centimeters (2.0 in.²); 92 percent YJ97 speed.

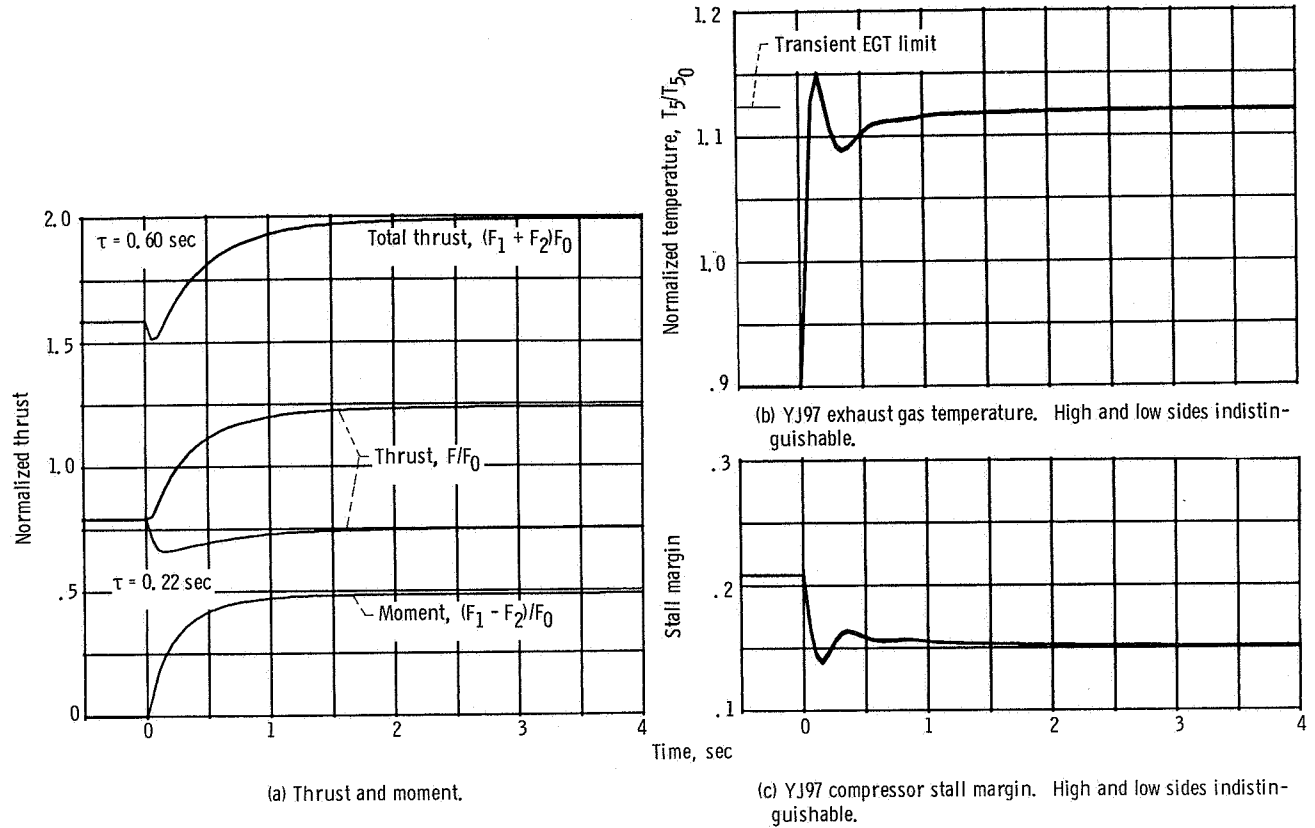
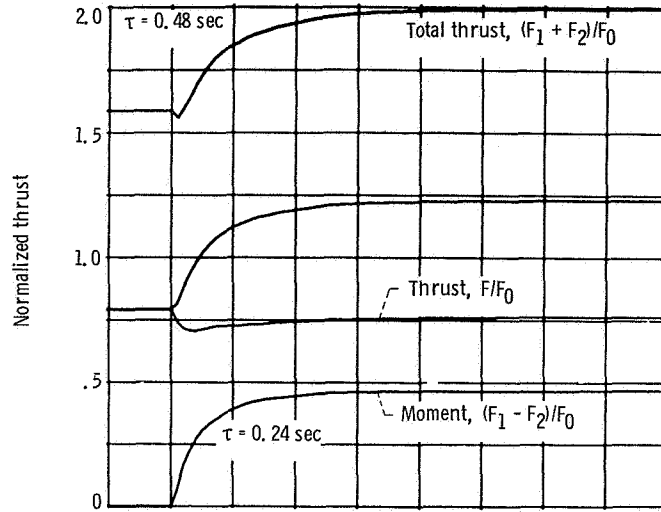
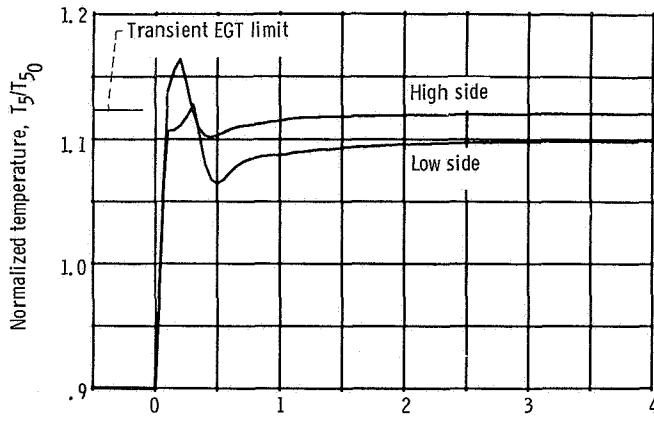


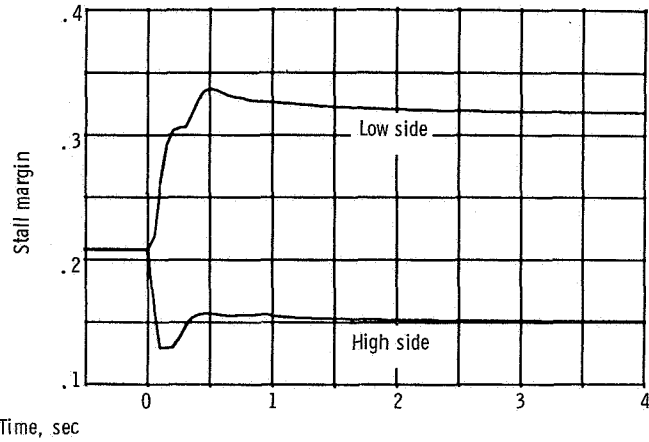
Figure 16. - ETC system response to 33.5° valve step and simultaneous YJ97 throttle step (from 95.8 to 101.5 percent speed).



(a) Thrust and moment.

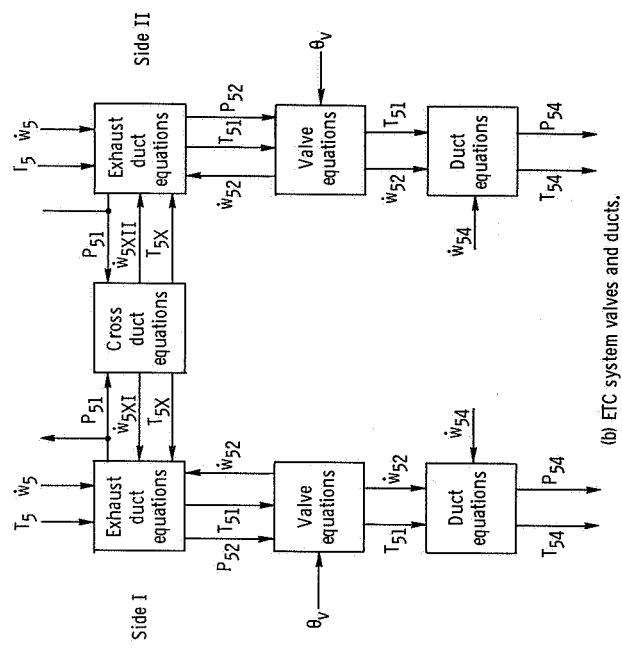


(b) YJ97 exhaust gas temperature.

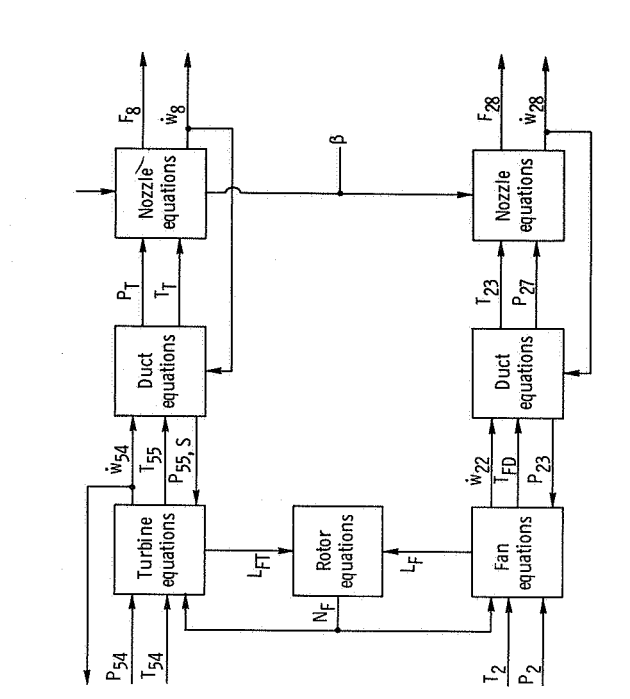


(c) YJ97 compressor stall margin.

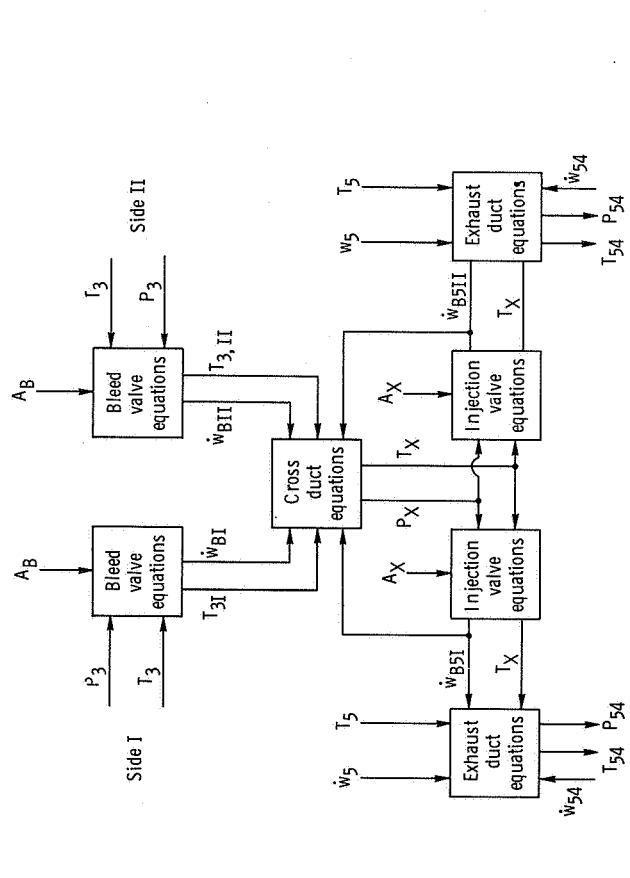
Figure 17. - Bleed system response to 19.1-square-centimeters (2.95-in.²) step in bleed valve area and simultaneous YJ97 throttle step (from 95.8 to 101.5 percent speed).



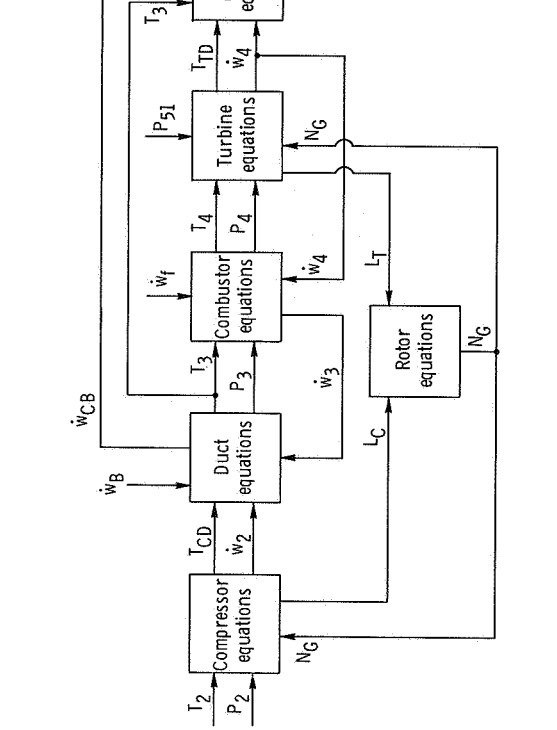
(a) YJ97 gas generator.



(b) ETC system valves and ducts.



(c) Compressor bleed system valves and ducts.



(d) LF460 fan.

Figure 18. - Analytical model.

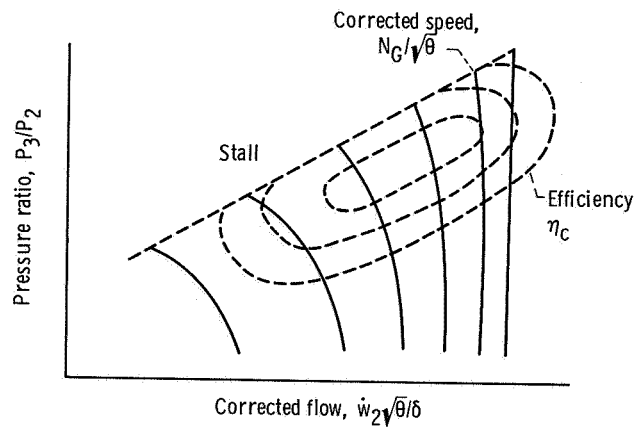


Figure 19. - YJ97 compressor map.

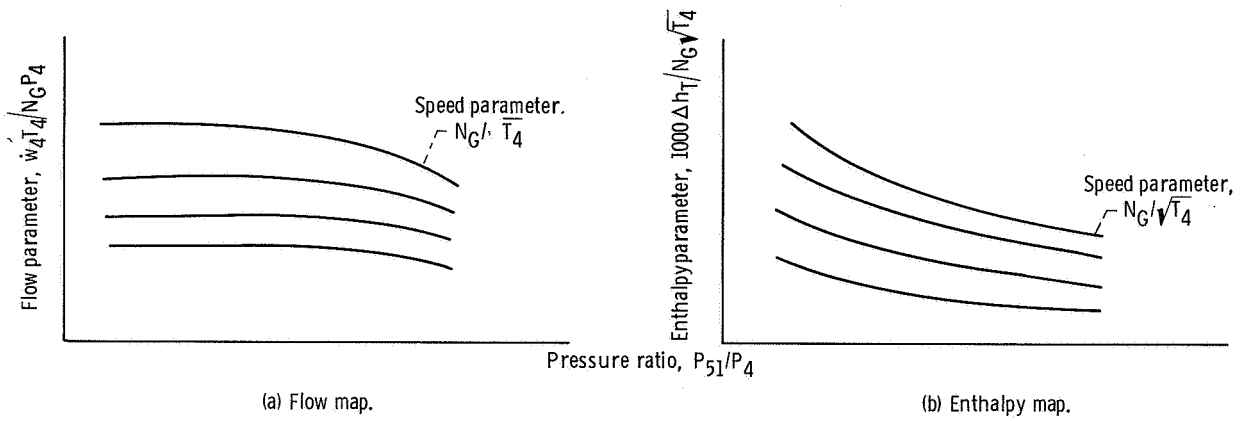


Figure 20. - YJ97 turbine maps.

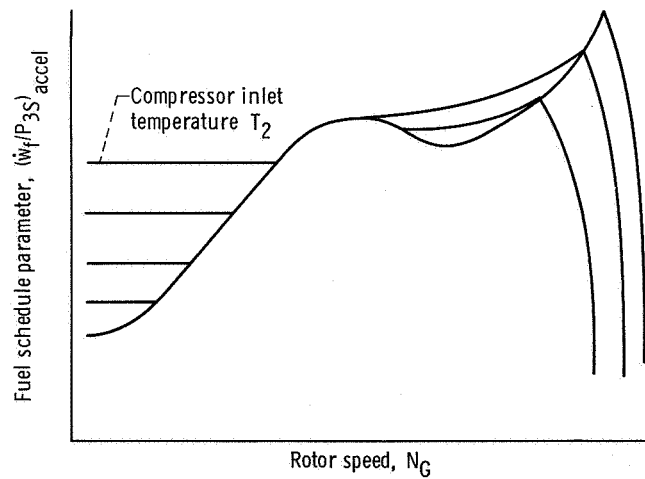


Figure 21. - YJ97 acceleration fuel flow schedule.

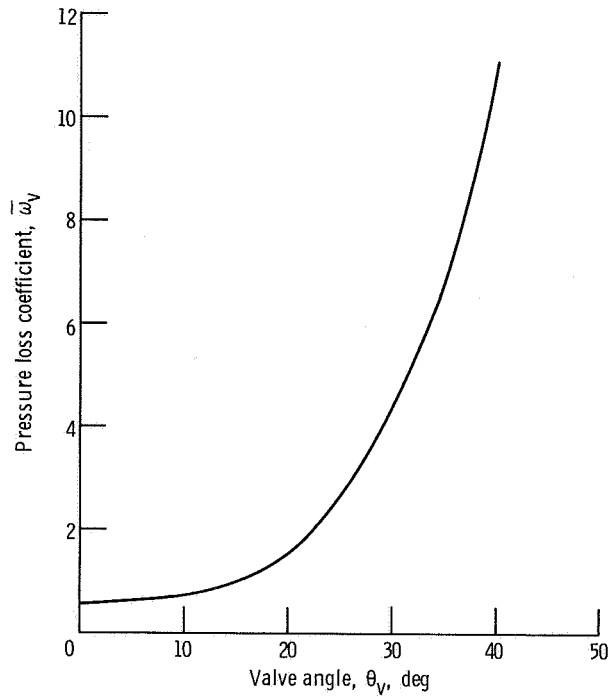


Figure 22. - Butterfly valve pressure loss (ref. 6).

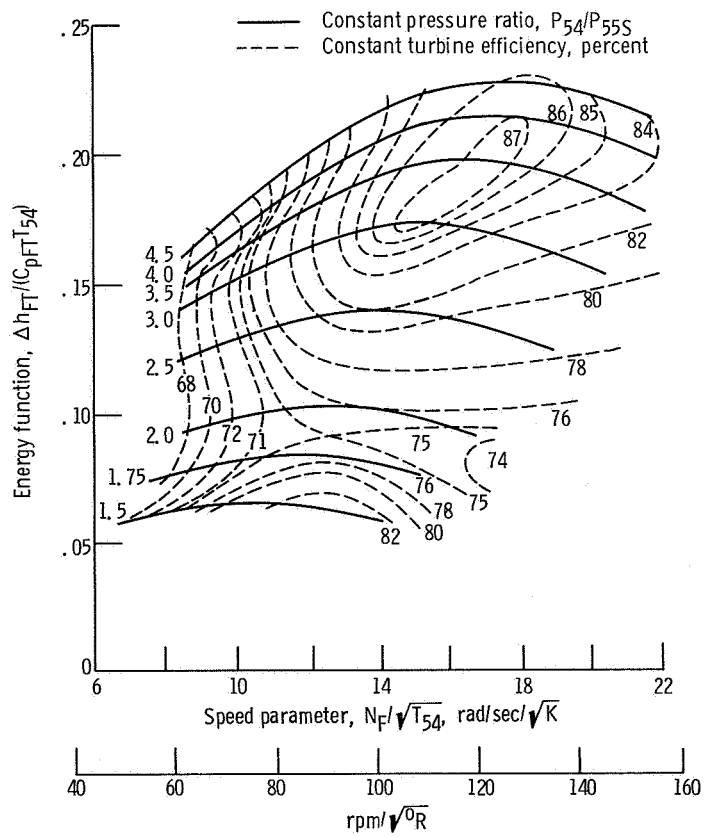


Figure 23. - LF460 estimated turbine map (ref. 9).

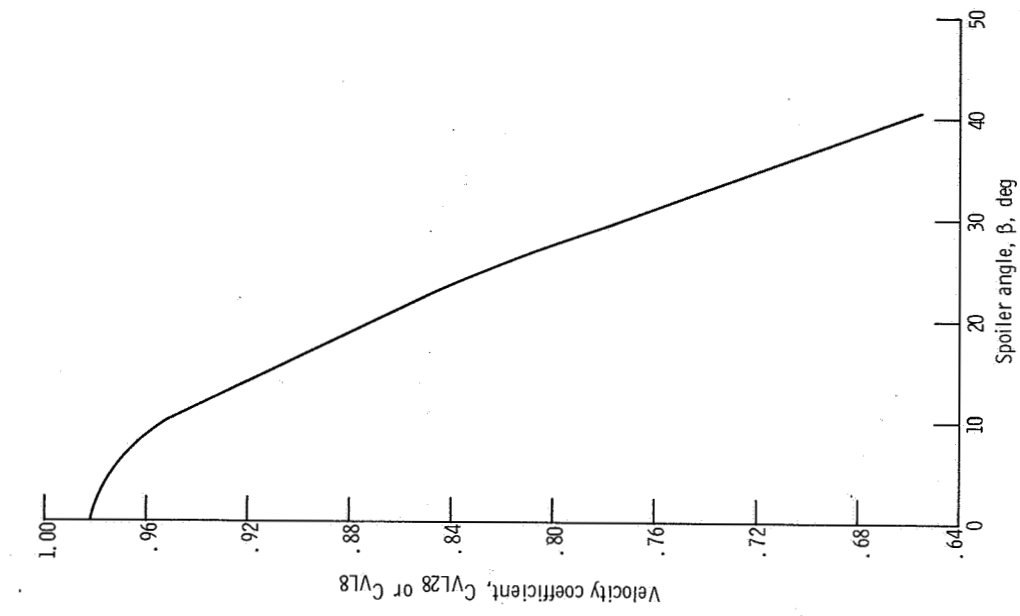


Figure 25. - LF460 exhaust velocity coefficient

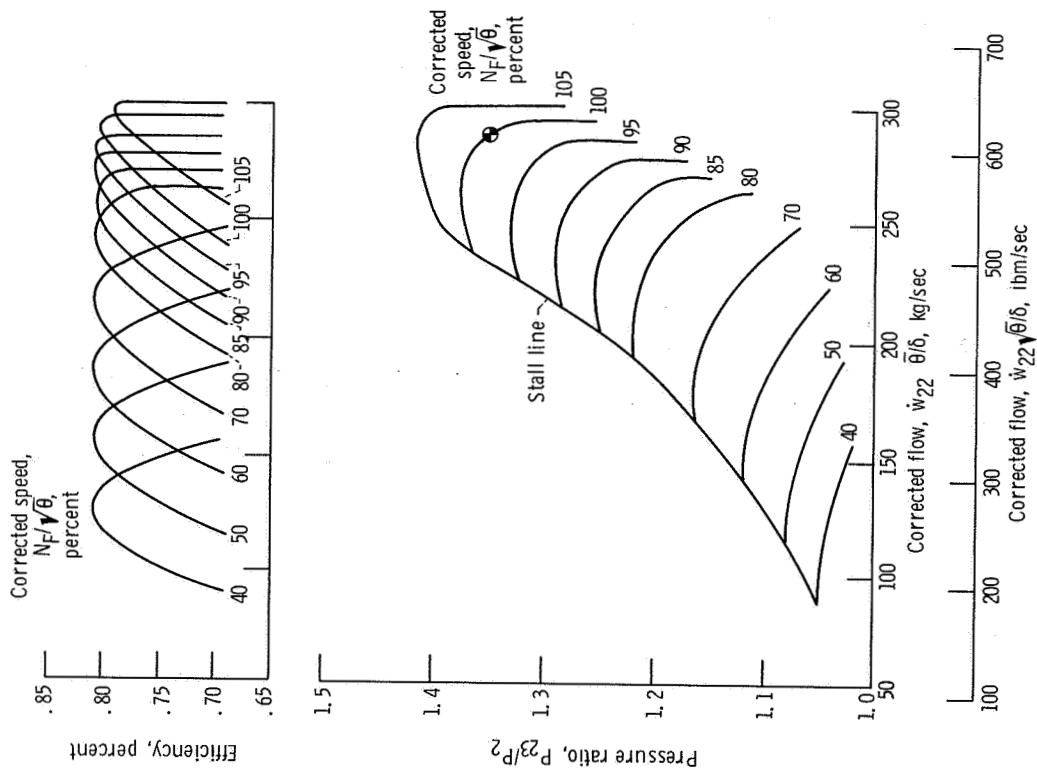


Figure 24. - LF460 estimated fan map (ref. 9).

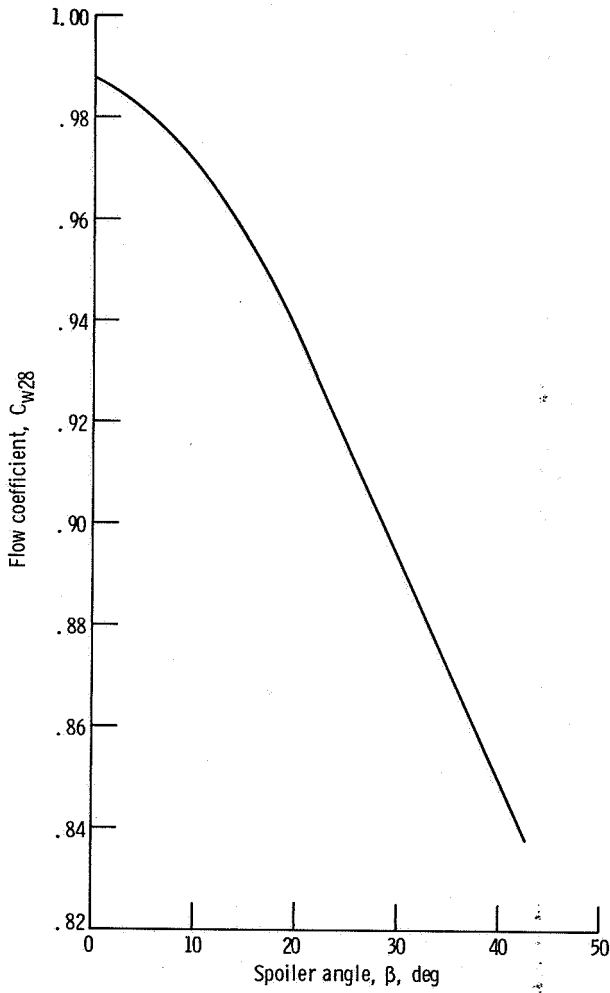


Figure 26. - LF460 fan exhaust flow coefficient.

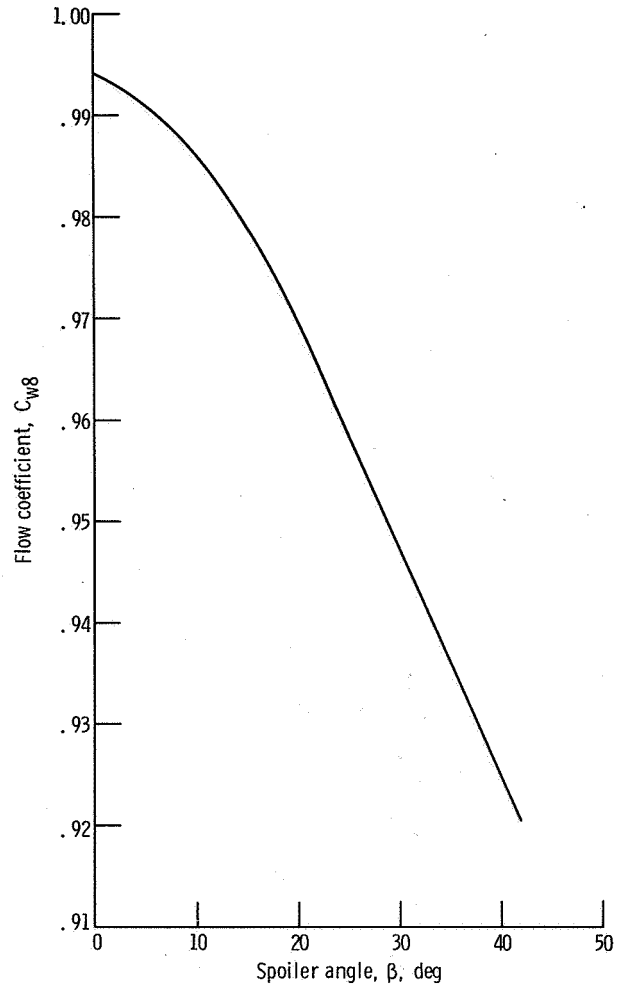


Figure 27. - LF460 turbine exhaust flow coefficient.